Analysis and Design for End Effects in Twisted Double Tees

Gregory Banks
Design Engineer
BERGER/ABAM Engineers
Federal Way, Washington

Laura N. Lowes, Ph.D.
Assistant Professor
Department of Civil Engineering
University of Washington
Seattle, Washington

John F. Stanton, Ph.D., P.E.
Professor
Department of Civil Engineering
University of Washington
Seattle, Washington

Prestressed concrete double tees are sometimes set on non-parallel supports to facilitate drainage; this practice induces twisting in the members. If the twist angle is large enough, cracks may occur in the flanges adjacent to the web-flange junction. This paper identifies the important modes of deformation and presents an analysis of the stresses and deformations caused by twisting. Local distortions of the cross section near the member ends are shown to play a pivotal role in bending and cracking of the flanges of double tees. A new theory of torsion that includes those deformations is developed, and a parametric study is carried out to show the effect of variations in the dimensions of the member. Finally, based on the new theory, the paper presents several graphs that facilitate the computation of the twist angle that causes cracking in a double tee of common dimensions.

Precast concrete double tees are designed to carry vertical load by bending, but they are sometimes also subjected to torsion. This twisting may occur intentionally, such as when the bearing supports at the two ends of the members are not parallel, a practice commonly used to facilitate drainage of a parking structure floor.

In this case, the stresses induced by the torsion are controlled by the magnitude of the imposed twist angle, which is defined by the difference between the slopes of the two supports. In other cases, the member may twist unintentionally by uneven lifting from the casting bed, storage conditions,

transportation on a flexible trailer, or other causes. Excessive twisting has been found to cause cracking in the flange.

Such cracking is unlikely to jeopardize the structural integrity of the member because the reinforcement provides the strength necessary to resist the design loads and becomes active primarily after the concrete cracks. However, cracking is generally undesirable from a serviceability standpoint, and the cracks may need to be sealed if the member remains untopped.

In the past, the prediction of cracking due to warping has largely been based on experience rather than analysis. This paper presents an analytical method that relates the peak flange stress to the twist angle of the member. Based on this approach, several graphs are developed that simplify implementation of that relationship. Note that selection of the maximum stress that should be allowed in practice or the acceptable extent of cracking are beyond the scope of the study.

Consider the case of a double tee bearing on non-parallel supports, with all four stems in contact with their supports, as shown in Fig. 1a. The total load can be broken down into two load cases, which may be superimposed. The first consists of a uniform gravity load applied to the member, which is supported on four hypothetical supports at the same level (see Fig. 1b). This load case induces bending but no torsion.

The second load case consists of removing one of the four supports and applying at that point a concentrated downward load that results in a deflection equal to the lack of parallelism in the real supports (see Fig. 1c). This second load case induces torsion and is the one of interest in this investigation.

At first glance, the problem appears to be a relatively straightforward case of St. Venant's torsion; that is, a single, prismatic element subjected to a constant torque with unrestrained warping. It is argued here, however, that the torque is applied at the ends of the member by means of vertical forces on the stems and that the distribution of stresses near the ends differs significantly from that predicted by St. Venant's torsion theory.

These end stresses are the primary cause of flange cracking. A method of analysis that incorporates both the St. Venant twisting of the member and the deformations of the flange is needed if the flange stresses near the end of the member are to be predicted.

PREVIOUS RESEARCH

Mack et al.[1] published a comprehensive state-of-the-art paper on the subject of warping caused by non-parallel supports. That paper treated the problem as one of pure St. Venant torsion, which induces only shear stresses, and developed an elegant numerical method for finding the exact torsional properties of the cross section by using Prandtl's soap-film analogy.[2]

From these properties, the shear stresses due to the applied torque and the highest shear stress at the web-flange junction were computed. Then, from this peak shear stress, the maximum normal stress was obtained for a variety of double tees subjected to a range of different twist angles.

A previous PCI-sponsored study conducted by The Consulting Engineers Group, Inc. (CEG)[3] addressed a wide range of issues related to the durability of parking structures, including warping of double tees. CEG conducted several three-dimensional finite element analyses (FEAs) of a double tee using solid ("brick") elements, which led to calculations of stresses in the flanges of the tees.

The results of that study include the distribution of principal stresses at one end of a member. Those stresses reach a maximum at the end of the member; that is, at the top of the flange at the web-flange junction at one web and at the bottom of the flange at the web-flange junction at the other web, as indicated in Fig. 2.

Stresses diminish with distance from the ends of the member. CEG identified these stresses as flange bending stresses rather than torsional shear stresses. A plot of maximum stress as a function of the "degree of warp" (i.e., the deflection of the one free support relative to the plane defined by the other three) was provided. However, the results of the linearly elastic FEA must have contained some scatter, because the predicted stresses for the 60 ft (18.3 m) double tee were represented by a bilinear curve that did not pass through the origin.
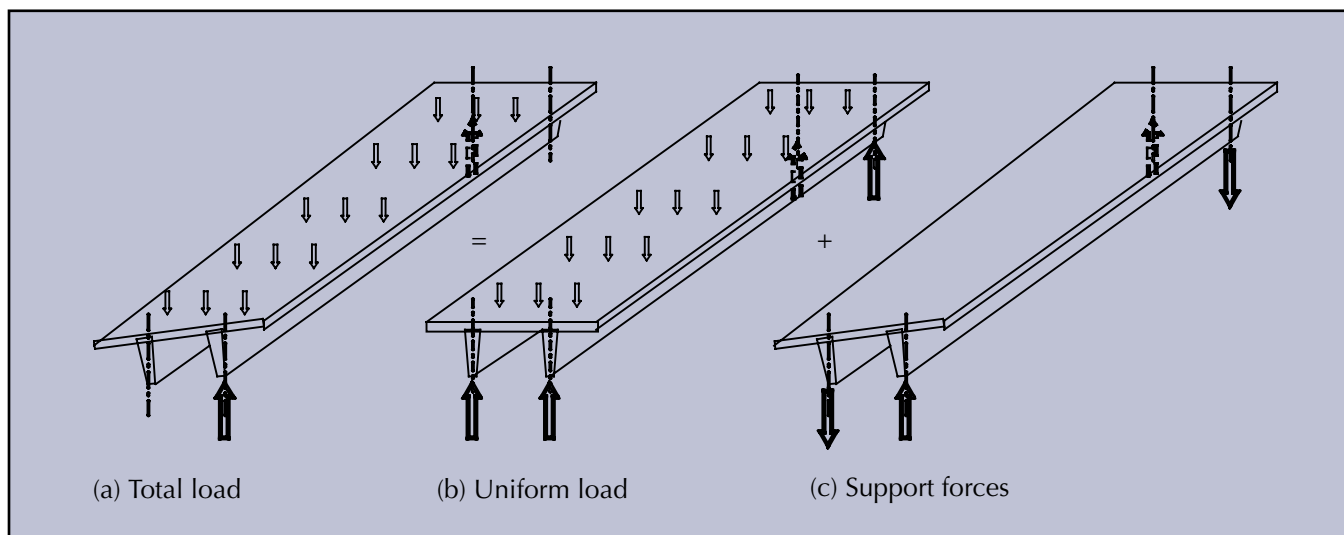

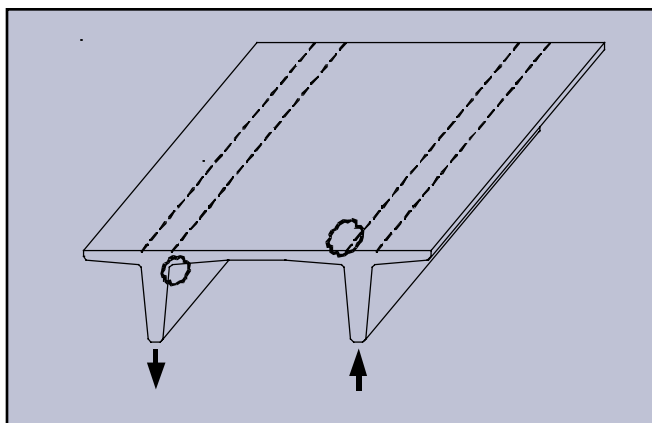Fig. 1. Support reactions on a double tee resting on non-parallel supports.

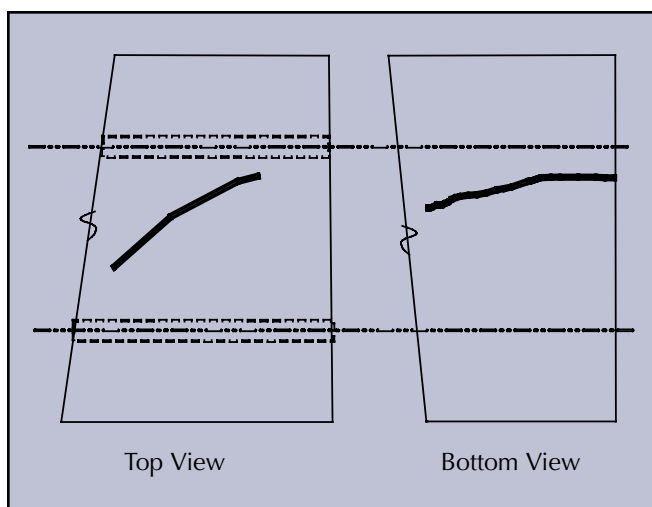Fig. 2. Locations of maximum stress due to twisting.

Top View   Bottom View

Fig. 3. Cracks in CEG double tee (from Mack et al.[1]).

In this paper, the notation 10DT24 is taken to mean a 10 ft (3.05 m) wide double tee with a clear web height below the flange of 24 in. (610 mm). The notation "+2" indicates a 2 in. (51 mm) thick flange, and "_60" means a 60 ft (18.3 m) span. Thus, a 12DT30+2_62 section has a 12 ft (3.66 m) member width, a 30 in. (762 mm) web depth below the flange, a 2 in. (51 mm) flange thickness, and a 62 ft (18.90 m) span.

This nomenclature follows the example of Mack et al.[1] but differs from that used by many practitioners. It is convenient here because it permits an easy definition of sections with the same stem geometry and fabricated in the same form, but with different flange thicknesses.

CEG also conducted field tests on a 47.0 and 60.5 ft (14.3 and 18.4 m) long pretopped 10DT24+4 section. Each member had, at each end, a 2 in. deep by 1 ft 11 in. wide (51 × 533 mm) recess in the flange spanning the entire 10 ft (3.05 m) width to accommodate a cast-in-place pour strip.

A longitudinal crack started at each web-flange junction at one end of the member and propagated toward midspan. One crack initiated in the top and one in the bottom of the flange, as shown in Fig. 3. In most cases, the crack turned inward from the web-flange junction toward the member centerline as it propagated away from the member end. With the exception of the fact that cracking occurred at only one end of the member, which may have been due to slight differences in

the boundary conditions for the loaded and simply supported ends of the member, the observed damage patterns were consistent with the results of the FEA.

The crack patterns observed by CEG suggest that the behavior at the ends of the specimen is dominated by the flange bending mechanism observed in their finite element model of a double tee. However, no such stresses are predicted by conventional models of torsion. The observed cracking and the results of the FEA suggest also that the flexural bending mechanism developed at the member ends gives way to a conventional torsional mechanism toward midspan of the member.

CLASSICAL TORSION THEORY

As a first step toward developing a model for predicting flange bending stresses, classical torsion theory[2] is reviewed and the need for an extension to the theory is established.

Closed sections (i.e., tubes) and solid sections can be analyzed for torsion using the simplest possible approach, originally developed by Barre de St. Venant.[4] For these sections, deformations are assumed to be caused by shear stresses alone. (This assumption is strictly true only in circular sections, but it causes very little error in most closed or solid sections.)

Points in the member do not displace longitudinally, so a cross section that is plane in the unstressed member remains plane under load. In other words, the cross section does not warp. In this case, the torque, $T(z)$, and the twist angle, $\phi(z)$, at any longitudinal location, z, are related by:

$$T(z) = GJ\phi'(z) \qquad (1)$$

where

T = torque
G = shear modulus
J = St. Venant torsion constant, defined by member geometry
ϕ = twist angle at location z
z = longitudinal coordinate

The prime (′) indicates differentiation with respect to z. In Eqs. (1) to (45), which describe the theory, the units are not restricted to any single system; they need only be consistent with each other.

In open sections, the assumption that plane sections remain plane can no longer be made because some longitudinal displacement occurs. A cross section that is plane in the unstressed member becomes nonplanar under load, and the cross section warps.

Accounting for the two different types of deformation (shear strains and longitudinal deformation) leads to two components of torque: one due to St. Venant shear stresses and one due to restraint-of-warping stresses. St. Venant shear stresses circulate around the individual segments (such as webs and flange) of the cross section but provide no net shear force.

The restraint-of-warping stresses lead to equal and opposite shear forces in the webs of members such as double tees. The couple formed by these web shear forces multiplied by the web spacing forms the component of torque associated with restraint of warping.

The total torque is the sum of these two components, and is related to the twist angle, $\phi(z)$, by:[2]

$$T(z) = GJ\phi'(z) - EC_w\phi'''(z) \qquad (2)$$

where
  E = Young's modulus of elasticity
  C_w = restraint-of-warping torsion constant, defined by member geometry

Eq. (2) is used widely to analyze open sections such as wide-flange steel sections, and might be expected to be suitable for double tees as well. However, it is shown below that an inconsistency occurs if the end torque is applied by a couple that consists of concentrated loads such as the support reactions.

Application of Classical Torsion Theory to Double Tees

In a member such as a uniformly loaded double tee, the torque is applied only at the member ends; thus, the total torque is constant along the member length. At the member ends, warping is unrestrained, so no longitudinal stresses can exist and the bi-moment, B, is zero. In a double tee, the bi-moment is given by the moment in each web multiplied by the distance between webs, and it is defined by:

$$B(z) = EC_w\phi''(z) \qquad (3)$$

where E, C_w, and ϕ are defined as in Eqs. (1) and (2).

The differential of the bi-moment with respect to z gives the component of torque in the member due to restraint of warping. Solving Eq. (2) for the case of constant torque and $\phi'' = 0$ at the ends shows that the restraint-of-warping torque is zero all along the member.

If the component of torque due to restraint of warping is zero along the entire length of the element, it follows that the St. Venant component of the torque is equal to the total torque and, therefore, is constant along the member. However, the end plane of the member is a free surface, so the shear stresses acting on it must be zero. Since these shear stresses define the St. Venant torque, the St. Venant torque also is zero at the member ends. If the St. Venant torque is constant along the length of the member and is zero at the ends, it must be zero everywhere else.

Therein lies the inconsistency in applying classical torsion theory to describe the behavior of a double tee loaded as shown in Fig. 1c. The torque components due to St. Venant's torsion and due to restraint-of-warping torsion must both be zero everywhere, yet the member is being twisted. Clearly, classical torsion theory, even allowing for warping of the cross section, does not describe fully the response of an open section such as a double tee.

In any member subjected to end forces alone, the distribution of stresses at the end may differ from that in the interior of the member even though the two have the same force or moment resultant. Examples are given by the shear stress distribution at the end of a beam that rests on a simple support and is subjected to vertical load, or by the case considered here of stresses due to unequal vertical forces acting on the stems of a double tee.

The total stress state at the end of a member may be thought of as the stress state in the interior of the member plus an additional set of local end stresses. St. Venant's principle (quite separate from his work on torsion) states that these local end stresses attenuate to negligible values at a distance from the end that is approximately equal to one member depth.

In many applications, these end effects are ignored, if for no other reason than the fact that they are difficult to calculate. In metal members, for example, this assumption may be justified because the cross-sectional dimensions are often much smaller than the length (in which case the end effects have little effect on the total twist angle of the member) and because any adverse local stresses that they may introduce are absorbed by small inelastic deformations.

However, the damage patterns in the double tees tested by CEG and the stress fields observed in the FEA that CEG performed suggest that the local end stresses cannot be neglected in the double tee problem; it is these stresses, rather than the St. Venant torsional shear stresses in the body of the member, that are the cause of the flange cracking. Thus, a modified model for torsion is needed in order to establish the magnitude of the local stresses.

DEVELOPMENT OF A NEW TORSION MODEL

The inconsistency in the classical torsion model described above can only be resolved by introducing a third source of deformation, in addition to the St. Venant shear deformations and the longitudinal (warping) deformations included in the classical model of Eq. (2). The cracking that occurred in the double tees tested by CEG suggests that this additional and previously unaccounted for deformation mode is associated with flange bending. Thus, it is proposed that the torsional behavior of a double tee be described by warping of the cross section and by two sources of twisting deformation (see Fig. 4).

The first of these twisting modes is a rigid body rotation of the cross section (see Fig. 4a), which is the deformation
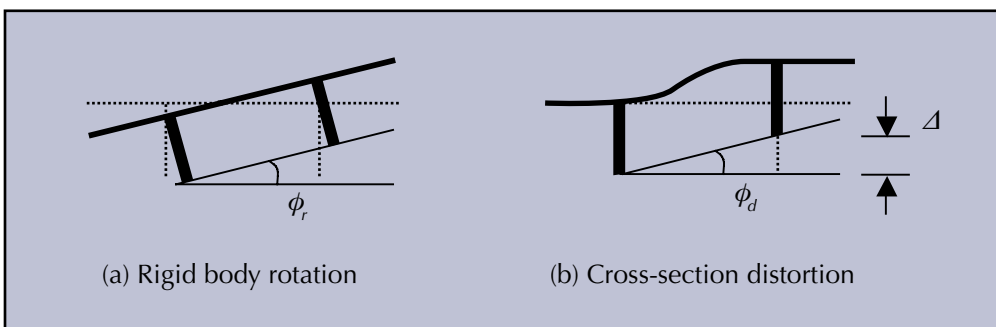

Fig. 4. Components of twist angle: (a) Rigid body rotation; (b) Cross-section distortion.

(a) Rigid body rotation   (b) Cross-section distortion

field that underlies St. Venant's torsion theory. The second is distortion of the cross section caused by transverse bending of the flange, which leads to vertical displacement of one web with respect to the other (see Fig. 4b).

It is expected that this second displacement field will be greatest near the ends of the member, where the torque is applied in a manner that is different from that envisaged in classical theory, and that it will diminish toward midspan. Additionally, the double tee webs remain parallel to their unstressed orientation, and all deformation occurs through flange bending, rather than web bending. This behavior may be explained as follows.

No horizontal forces act on the webs, so they experience no out-of-plane bending. Symmetry then requires that the webs remain parallel to each other. If they both rotate through the same angle, that rotation forms the rigid body rotation associated with the St. Venant torsion and is accounted for separately. Thus, for the component of twisting associated with the cross-section distortion, the webs remain vertical.

The total torsional deformation of a double tee may be defined as the sum of the two components shown in Fig. 4:

$$\phi_t(z) = \phi_r(z) + \phi_d(z) \tag{4}$$

where
- ϕ_t = total twist angle
- ϕ_r = twist angle due to rigid body rotation of cross section
- ϕ_d = twist angle due to cross-section distortion

The total torque, T_t, consists of a St. Venant component, T_{SV}, and a restraint-of-warping component, T_{RW}:

$$T_t(z) = T_{SV}(z) + T_{RW}(z) = GJ\phi_r'(z) - EC_w\phi_t'''(z) \tag{5}$$

where the St. Venant torque depends on the ϕ_r component of the twist angle alone, because this is the only deformation that leads to torsional shear stresses.

By contrast, restraint-of-warping torque is associated with in-plane bending deformation of the webs, which is related through geometry to the total twist angle. Combining Eqs. (4) and (5) leads to:

$$T_t(z) = [GJ\phi_r'(z) - EC_w\phi_r'''(z)] - EC_w\phi_d'''(z) \tag{6}$$

Eq. (6) is identical to the classical torsion model [Eq. (2)], with the exception that an additional term accounts for torque due to cross-section distortion, which is necessary to model the response near the member ends.

To solve the torsion problem defined by Eq. (6), an additional equilibrium equation is required to eliminate the additional unknown, ϕ_d. It is given by considering moment equilibrium about the longitudinal axis of a short section of the web, as shown in Fig. 5. The difference between the St. Venant torques at the two ends of the web element is equilibrated by the moment from the flange bending:

$$m_f(z)dz + dT_{SVw}(z) = 0 \tag{7a}$$

or

$$m_f(z) + \frac{d}{dz}T_{SVw}(z) = 0 \tag{7b}$$

where
- m_f = transverse flange moment per unit length along member
- T_{SVw} = St. Venant torque in one web

Assuming the flange responds as a plate subjected to bending about a single axis, the flange moment is defined as:

$$m_f(z) = \frac{6D_f\Delta(z)}{s^2} = \frac{6D_f}{s}\phi_d(z) \tag{8}$$

where
- Δ = vertical offset of the two webs (see Fig. 4b)
- s = center-to-center web spacing
- D_f = bending stiffness of flange per unit length of double tee
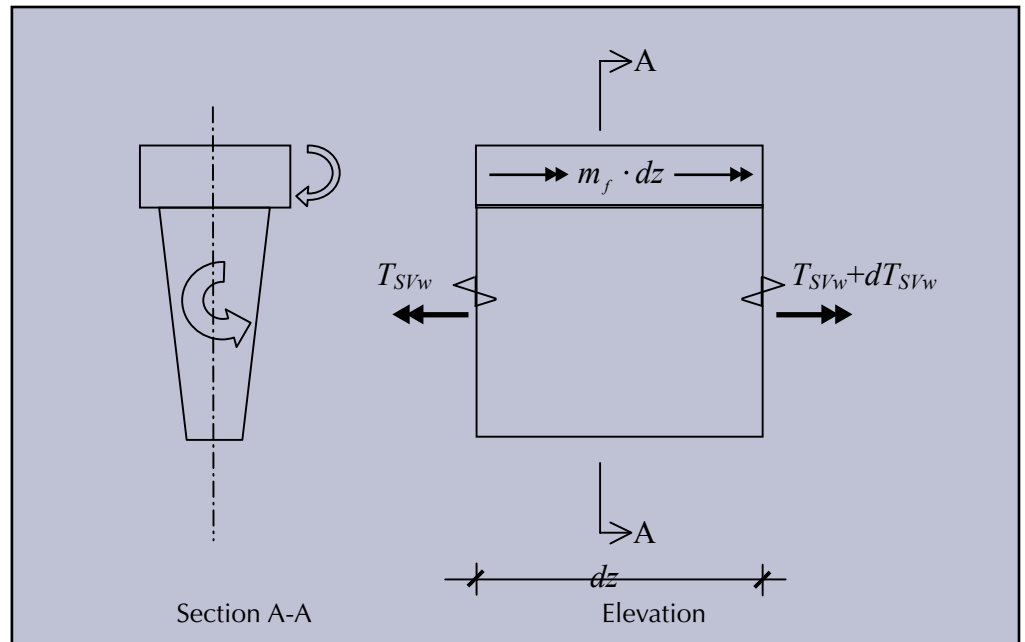- $= \dfrac{Et_f^3}{12(1 - \nu_c^2)}$
- t_f = flange thickness

Fig. 5. Equilibrium of web segment.

Section A-A   Elevation

ν_c = Poisson's ratio for concrete

The St. Venant web torque, T_{SVw}, is given by:

$$T_{SVw}(z) = GJ_w\phi_r'(z) \qquad (9)$$

where J_w is the St. Venant torsion constant for one web.

Substituting Eqs. (8) and (9) into Eq. (7b) yields:

$$\phi_d(z) = \frac{-sGJ_w}{6D_f}\phi_r''(z) \qquad (10)$$

Eq. (10) provides the additional information needed to eliminate the unknown, ϕ_d, from Eq. (6).

Substituting Eq. (10) into Eq. (6) and setting the derivative of the total torque equal to zero, since the torque is constant along the length of the member, results in:

$$GJ\phi_r''(z) - EC_w\phi_r^{iv}(z) + GC_d\phi_r^{vi}(z) = 0 \qquad (11)$$

where

$$C_d = \frac{sJ_wEC_w}{6D_f} \qquad (12)$$

The quantity C_d may be thought of as a torsional member property that is associated with distortion of the cross section. It has units of length to the eighth power. Note that the variable D_f contains Young's modulus of elasticity, E, so the material property constants on the right hand side of Eq. (12) cancel, leaving the units of C_d in terms of length alone.

To facilitate its solution, Eq. (11) is rearranged as follows:

$$\phi_r^{vi}(z) - 2\nu^2\phi_r^{iv}(z) + 2\nu^2\lambda^2\phi_r''(z) = 0 \qquad (13)$$

where

$$\lambda^2 = \frac{GJ}{EC_w} \qquad (14)$$

$$\nu^2 = \frac{3D_f}{sGJ_w} \qquad (15)$$

Note that both λ and ν have units of length^{-1}.

Six boundary conditions are needed to solve the sixth order differential equation defined by Eq. (13). In most cases, the double tee problem is anti-symmetric. If the origin is taken at midspan of the double tee, the six boundary conditions are:

$$\phi_t(\pm L/2) = \pm\phi_0/2 \text{ (known twist angle at each end) (16a)}$$

$$\phi_r'(\pm L/2) = 0 \text{ (no St. Venant torque at each end)} \quad (16b)$$

$$\phi_t''(\pm L/2) = 0 \text{ (no bi-moment at each end)} \qquad (16c)$$

where ϕ_0 is the total torsional rotation of one end of the member relative to the other.

SOLUTION STRATEGIES

The problem defined by Eqs. (13) to (16) may be solved analytically (i.e., in closed form) or by using the finite difference (FD) method. Both methods were used here to verify that the solutions are correct. The analytical solution is presented first, followed by the FD solution.

Analytical Solution

The torsion problem defined by Eqs. (13) to (16) may be solved using traditional analytical methods. A report by the authors[5] provides a detailed discussion of the analytical solution process; only the primary results are provided here.

At the member end ($z = L/2$), the rotations ϕ_r, ϕ_d, and ϕ_t are given by:

$$\phi_r\left(\frac{L}{2}\right) = \left(\frac{\phi_0/2}{1 + 1/c_t}\right) \qquad (17a)$$

$$\phi_d\left(\frac{L}{2}\right) = \left(\frac{\phi_0/2}{1 + c_t}\right) = \frac{\phi_r(L/2)}{c_t} \qquad (17b)$$

$$\phi_t\left(\frac{L}{2}\right) = \phi_0/2 \qquad (17c)$$

where c_t is a dimensionless parameter defined as:

$$c_t = \frac{c_\eta}{\varrho} \qquad (18)$$

$$c_\eta = \frac{\left(\frac{\eta_1 L}{2}\right)}{\tanh\left(\frac{\eta_1 L}{2}\right)} - \frac{\left(\frac{\eta_2 L}{2}\right)}{\tanh\left(\frac{\eta_2 L}{2}\right)} \qquad (19)$$

$$\eta_{1,2} = \nu\sqrt{1 \pm \varrho} \qquad (20)$$

$$\varrho^2 = \left(1 - \frac{2\lambda^2}{\nu^2}\right) \qquad (21)$$

Eqs. (17a) to (17c) show that c_t is the critical parameter that controls the behavior of the system. Its value depends on the two dimensionless variables λL and νL, where λ^2 is the ratio between the St. Venant and restraint-of-warping torsional stiffnesses [Eq. (14)], and ν^2 defines the bending stiffness of the flange relative to the St. Venant torsional stiffness of the web [Eq. (15)]. All the other variables, such as ϱ and η, are functions of the dimensionless variables λL and νL.

For physical reasons [i.e., Eq. (17)], c_t must always be real. However, ϱ [Eq. (21)] may be real or imaginary. If ϱ is real (typically in a thick-flanged member), then η_1 and η_2 are also real, and Eqs. (18) and (19) can be evaluated directly. If ϱ is imaginary, then c_η must also be imaginary, and Eqs. (18) and (19) cannot be computed using a conventional calculator. For the case of imaginary ϱ and c_η values, the value of c_t [Eq. (18)] may be computed without the use of complex numbers as follows:

$$c_t = \frac{c_\eta}{\varrho} = \frac{2}{\mu}\left(\frac{w\sinh(2u) - u\sin(2w)}{\cosh(2u) - \cos(2w)}\right) \qquad (22)$$

where

$$\mu = \varrho/i = \|\varrho\| \qquad (23a)$$

$$i = \sqrt{-1} \qquad (23b)$$

$$r = \frac{\nu L}{2}\sqrt[4]{4 + \mu^2} \qquad (23c)$$

$$\theta = \frac{1}{2} \arctan(\mu) \tag{23d}$$

$$u = r\cos\theta \tag{23e}$$

$$w = r\sin\theta \tag{23f}$$

Fig. 6 shows c_t as a function of λL for different νL values. Because the calculation of c_t is moderately complicated, and in some cases involves complex numbers, developing a simpler approximation is desirable. The variations of c_t with λL and νL shown in Fig. 6 suggest that a linear approximation may be possible. The best-fit linear function of λL and νL was found to be:

$$c_t \approx (0.7147 - 0.0068\lambda L)\nu L - (0.9062 + 0.1005\lambda L) \tag{24}$$

In Fig. 6, the exact values of c_t are shown as symbols without lines and labeled νL, and the approximations are shown as straight lines without symbols and labeled νL_{app}. The fit appears good, and the mean error is 0.5 percent.

Eq. (17b) shows that a value of $c_t \gg 1.0$ indicates that only a small proportion of the total end twist angle is attributable to cross-section distortion, and $c_t = 0$ implies that the entire twist angle is due to distortion. Fig. 6 shows that c_t is much more sensitive to νL than to λL.

This finding can be explained physically by the fact that a small νL value is associated with thick webs, a thin flange, and a short member, in which case distortion of the cross section occurs relatively easily. By contrast, a large λL occurs when the St. Venant torsion constant is much larger than the restraint-of-warping constant, C_w, which typically occurs in long members, or those with short webs and thick flanges.

The relationship between these characteristics, and thus λL, and flange bending is weaker.

Finite Difference Solution

Development of the closed-form solutions requires considerable algebraic manipulation and gives rise to the possibility of error, so the problem defined by Eqs. (13) to (16) was solved also using the FD method in order to verify the closed-form results.

To develop the FD solution, the variable ϕ_r, which in Eq. (13) is a continuous function of z, is discretized along the length of the member. The variable $(\phi_r)_j$ is introduced to represent the value of ϕ_r at node j, which is located along the length of the member. Solution of the discretized problem requires calculation of $(\phi_r)_j$ at a total of n nodes.

The equilibrium requirement defined by Eq. (13) must be satisfied at each node:

$$(\phi_r^{vi})_j - 2\nu^2(\phi_r^{iv})_j + 2\nu^2\lambda^2(\phi_r'')_j = 0 \tag{25}$$

The derivatives of ϕ_r that appear in Eq. (25) are defined using the centered finite divided difference relationship, for example:

$$(\phi_r'')_j \approx \frac{1}{h^2}\left[(\phi_r)_{j+1} - 2(\phi_r)_j + (\phi_r)_{j-1}\right] \tag{26}$$

where h is the distance between adjacent nodes.

The centered finite difference relationship is more accurate than a forward or backward finite divided difference, but applying this relationship over the entire length of the member requires the introduction of extra nodes located outside the boundaries of the original domain. For example, to compute
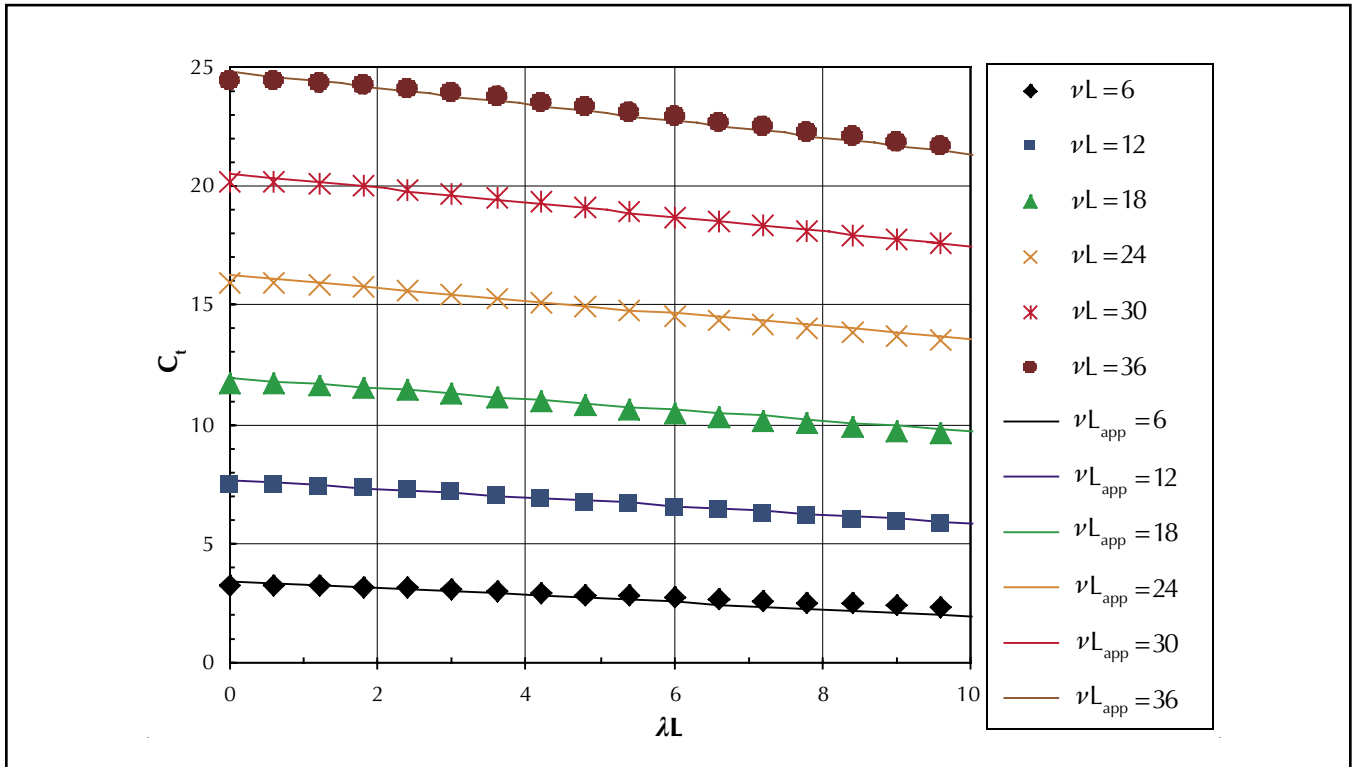

Fig. 6. Values of c_t versus λL.

the second derivative at the first node, $j = 0$, in the original domain requires the addition of node $j = -1$ so that $(\phi_r)_{-1}$ can be used in Eq. (26). The addition of extra nodes could have been avoided by using forward and backward divided difference relationships at the boundaries, but that approach was not used here.

Use of the centered finite divided difference relationships to define the derivatives in Eq. (13) results in a system of $n + 6$ equations that must be solved for the $n + 6$ unknown values of $(\phi_r)_j$, where the additional six unknown values of $(\phi_r)_j$ result from the use of nodes outside the domain boundaries and the additional six equations come from imposing the previously specified boundary conditions. The equations are expressed as:

$$A\Phi = y \qquad (27)$$

where A is a banded matrix of coefficients, Φ is the vector of unknown values of $(\phi_r)_j$, and y is a vector that contains mostly zeros, but also the applied twist angle.

The finite difference problem was solved using MATLAB.[6] Meshes with up to 769 equally spaced nodes were used to verify convergence of the solution. Although finer meshes reduced the truncation error in the finite difference approximation, they also led to larger round-off errors as the matrix A became increasingly ill-conditioned. These round-off errors were manifested by differences between the rotations at each end of the double tee, which should be equal and opposite, but in practice differed by increasingly large amounts as the mesh was refined.

The compromise that was finally selected was to use 289 nodes along the member. This choice led to a difference between the end rotations of less than 0.1 percent, and also led to a mesh of approximately the same size as that used for the FEA (to be described later).

Fig. 7 compares the analytical (solid lines) and finite difference (dashed lines) solutions for $\phi_r(z)$ and $\phi_d(z)$, using the three double tees whose geometric properties are defined in Table 1. In each case, only half the span is shown because the response is anti-symmetric.

Fig. 7 also shows the results of FEAs (symbols but no line) that are discussed later. The data are normalized by dividing the individual twist angle components by the total twist angle of one end relative to the other. The analytical and finite difference solutions are virtually indistinguishable, suggesting that the analytical solution to Eq. (13) is correct.

THE TORSIONAL RESPONSE OF DOUBLE TEES

The analytical solution provides a basis for computing two quantities of interest to the engineer: the flange bending moment and the true torsional stiffness of a double tee. These topics are discussed in the following sections.

Flange Bending Moment

The distribution of the flange bending moment along the length of the member is of particular interest, as it is this moment that causes high tensile stresses at the web-flange inter-

face and cracking of the double tee. The exact distribution of flange bending moment along the member depends on the section properties, but several general observations can be made that help explain the nature of the behavior.

Using Eqs. (8) and (17b), the flange moment at the end of the member (where it is maximum) is:

$$m_{f,max} = \frac{6D_f}{s}\phi_d = \frac{6D_f}{s}\left(\frac{\phi_0/2}{1 + c_t}\right) \qquad (28)$$

Because the flange moment is directly proportional to the distortion twist angle, ϕ_d, the distribution of ϕ_d along the member length is considered here as a proxy for the flange moment. Fig. 7 shows the distribution of ϕ_r and ϕ_d as functions of z/L, the distance from midspan normalized with respect to the total span length, for three 10DT24 cases. In each case, only half of the member is shown, since the response is symmetric.

Figs. 7a to 7c are arranged in decreasing order of the ratio of out-of-plane flange stiffness to in-plane web stiffness. For the 4 in. (100 mm) thick flange and 60 ft (18.3 m) span (Fig. 7a), ϕ_d is significant only near the ends of the member, where $z/L = 0.5$. This is so because the flange is relatively stiff in bending and rapidly suppresses any distortion of the cross section at locations distant from the support. Over about the central 80 percent of the member, the behavior is essentially pure St. Venant torsion.

By contrast, Fig. 7b shows that the 2 in. (51 mm) flange is much less stiff in transverse bending, so the cross-section distortions do not die out so rapidly. (In this case, the one member depth suggested by St. Venant for attenuation of local end effects significantly underestimates the real value.)

For the 10DT24 with a 2 in. (51 mm) flange spanning 10 ft (3.1 m), shown in Fig. 7c, the flange is very flexible compared with the webs, so the twisting is strongly dominated by the cross-section deformation component, ϕ_d. The webs remain essentially straight and undergo rigid body motions, whereas the flange warps into a hyperbolic paraboloidal shape. The "end effects" exist throughout the member, and not even at midspan do the stresses reduce to the St. Venant shear stresses alone.

Fig. 8 shows the corresponding distributions of torque components along the member, normalized with respect to the total applied torque. For clarity, results are shown from the analytical solution alone. As with Fig. 7, the FD values are essentially identical. In all cases, the torque at the member end is carried by the restraint-of-warping component alone, because the St. Venant torsional shear stresses, and thus the St. Venant torque, are zero there. (The explanation for the

Table 1. Properties of double tees used in analyses.

Double tee designation	Span (ft)	b_f (in.)	t_f (in.)	s (in.)	h_w clear (in.)	t_w top (in.)	t_w bot (in.)
10DT24+4_60	60	120	4	60	24	8*	5*
10DT24+2_60	60	120	2	60	24	8*	5*
10DT24+2_10	10	120	2	60	24	8*	5*

* 6.5 in. used in comparisons with FEAs.
Note: 1 in. = 25.4 mm; 1 ft = 0.305 m.

inconsistency described previously is that ϕ_t'' is indeed zero at the member end, but the individual components ϕ_r'' and ϕ_d'' are not.)

Also, the restraint-of-warping torque, T_{RW}, diminishes at sections away from the end, but changes sign so that, at midspan, both components of torque exist but have opposite signs. Because the two components of torque have different signs, the St. Venant component is larger than the total applied torque.

Calculations of shear stress that are based on the presence of St. Venant torque alone will result in low estimates of the true shear stress. In Fig. 8a, the restraint-of-warping torque

has almost disappeared at midspan, but in Figs. 8b and 8c it never disappears, but rather provides a substantial contribution over the whole length.

The behavior is similar but not identical to that of a beam-on-elastic-foundation[7] in which the web of the double tee may be thought of as the beam and the flange as the elastic foundation. The local distortion of the cross section at the member end involves significant bending of the "beam" near the loading point (i.e., the support of the double tee), which disappears as a result of the continuously distributed forces imposed on it by the "foundation."

It is interesting to note that, at least in the case of the long, thick-flanged member shown in Fig. 8a, the flange bending moment changes sign and oscillates, thereby mimicking the distribution of the foundation forces in a typical beam-on-elastic-foundation system. The oscillations have little significance in practice because they are small and occur far away from the point of maximum flange moment.

Torsional Stiffness of Double Tees

The flange bending moment and stress are of paramount interest in evaluating the potential for cracking. There may be situations, however, in which the effect of cross-section distortion on torsional stiffness also is of interest.

Most structural analysis software (e.g., SAP2000[8]) models the torsional stiffness of a component using the assumption of pure St. Venant torsion. This may be unconservative if cross-section distortion is significant. Here, two approaches are proposed for including the additional torsional flexibility resulting from cross-section distortion in a structural analysis.

The total torque on the member can be computed using Eq. (5) in terms of the rotation angles $\phi_r(z)$ and $\phi_t(z)$. The resulting relationship between the total twist angle and the total torque is:

$$\phi_0 = \frac{T_t L}{GJ}\left(1 + \frac{1}{c_t}\right) \qquad (29)$$

This may be compared with the twist angle, $\phi_{0,SV}$, that arises from the use of the St. Venant model alone:

$$\phi_{0,SV} = \frac{T_t L}{GJ} \qquad (30)$$

Thus, for a given torque, the additional twist angle due to flange bending is:

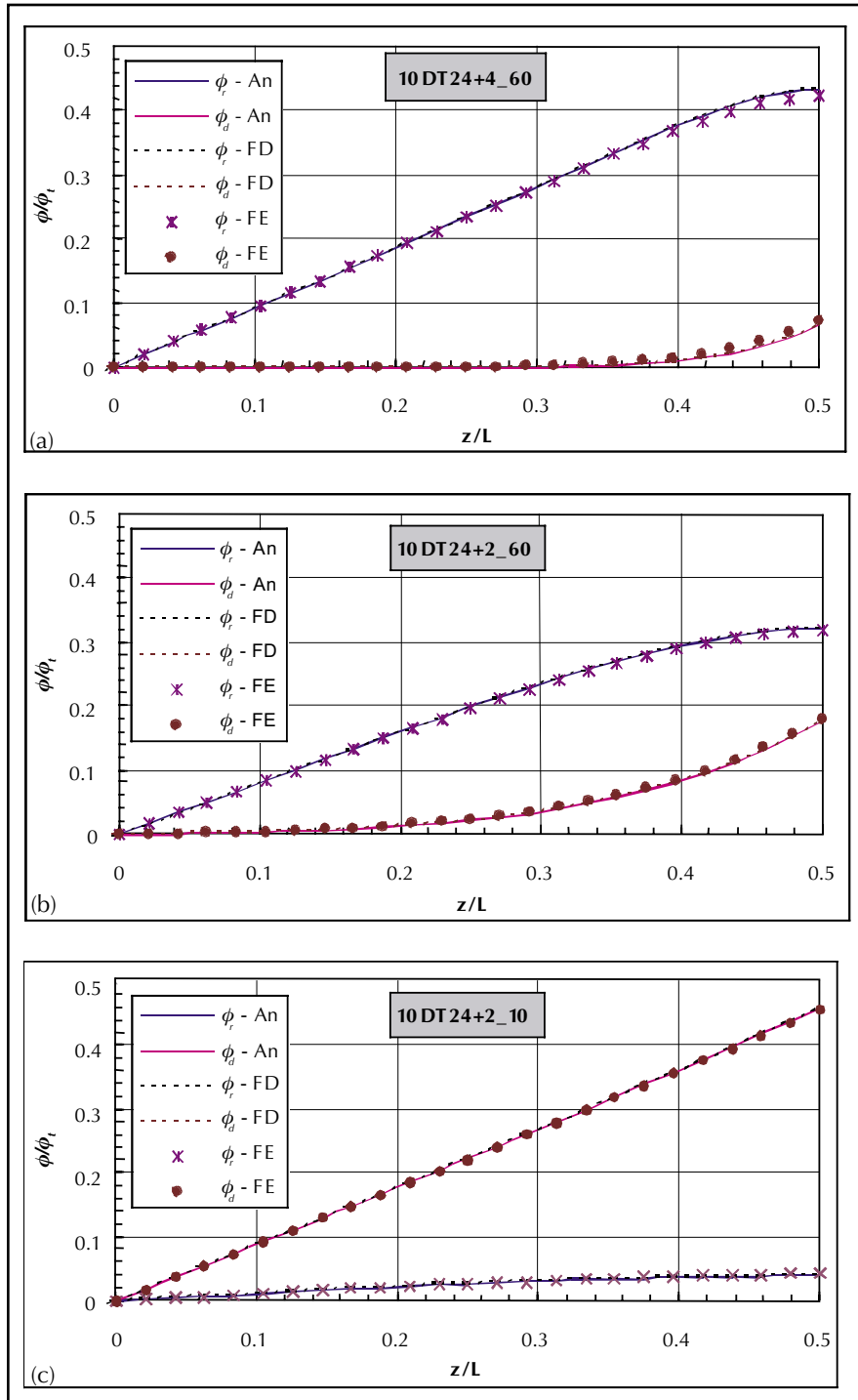$$\phi_{0,add} = \phi_0 - \phi_{0,SV} = \frac{1}{c_t}\frac{T_t L}{GJ} \qquad (31)$$

Fig. 7. Normalized ϕ versus z/L for three double tees: (a) 10DT24+4_60, (b) 10DT24+2_60, and (c) 10DT24+2_10.

This additional twist angle may be thought of as being supplied by a torsional spring, in series with the St. Venant model of the member. Its stiffness is:

$$K_{\theta,end} = \frac{T_t}{\phi_{0,add}} = c_t \frac{GJ}{L} \qquad (32)$$

The additional flexibility, defined by the inverse of $K_{\theta,end}$, can be evaluated approximately in extreme cases, such as for very long or very short members, to verify that Eq. (32) displays the appropriate asymptotic behavior. The critical dimensionless variable is c_t.

Eqs. (29) and (32) suggest that two approaches are possible for modeling the torsional stiffness of an element that exhibits cross-sectional distortion. One approach is to use an effective torsional constant, GJ_{eff}, for the element, defined by:

$$GJ_{eff} = GJ\left(\frac{c_t}{1+c_t}\right) \qquad (33)$$

A second approach is to add a rotational spring with stiffness $K_{\theta,end}$, as defined by Eq. (32), at one end of the member.

VERIFICATION OF MODEL USING FEA

The fact that the closed form and finite difference solutions to the problem give essentially identical results suggests that those solutions are both correct. However, to be useful in practice, the analytical model represented by Eq. (13) and its underlying assumptions must be shown to represent adequately the behavior of the real structure.

The principal assumption used is that the total twist angle can be modeled by the two terms ϕ_r and ϕ_d, and that they can be computed using Eqs. (4) to (10). This question was studied by conducting a series of finite element analyses and comparing the results with those of the analytical model.

An FE model of a 10DT24 section was created in SAP2000[8] using shell elements. Shell elements do not have an explicit representation of thickness, so elements were placed at the centerlines of the flange and webs of the double tee. Thus, the geometry of the elements did not have to be modified to simulate the web-flange intersection.

Shell elements were chosen because they represent the primary mechanisms that determine the response of the structure, but have less computational cost than solid elements. Further

analysis using solid elements to simulate better the finite web-flange intersection region and the tapered webs is possible but is beyond the scope of this study.

The shell elements were defined as having both membrane and bending stiffness. Analyses were conducted using both a thick-plate formulation, in which out-of-plane shear deformation is simulated, and a thin-plate formulation, in which it is neglected. The results of these two analyses were almost identical with the exception of the stress field at the very ends
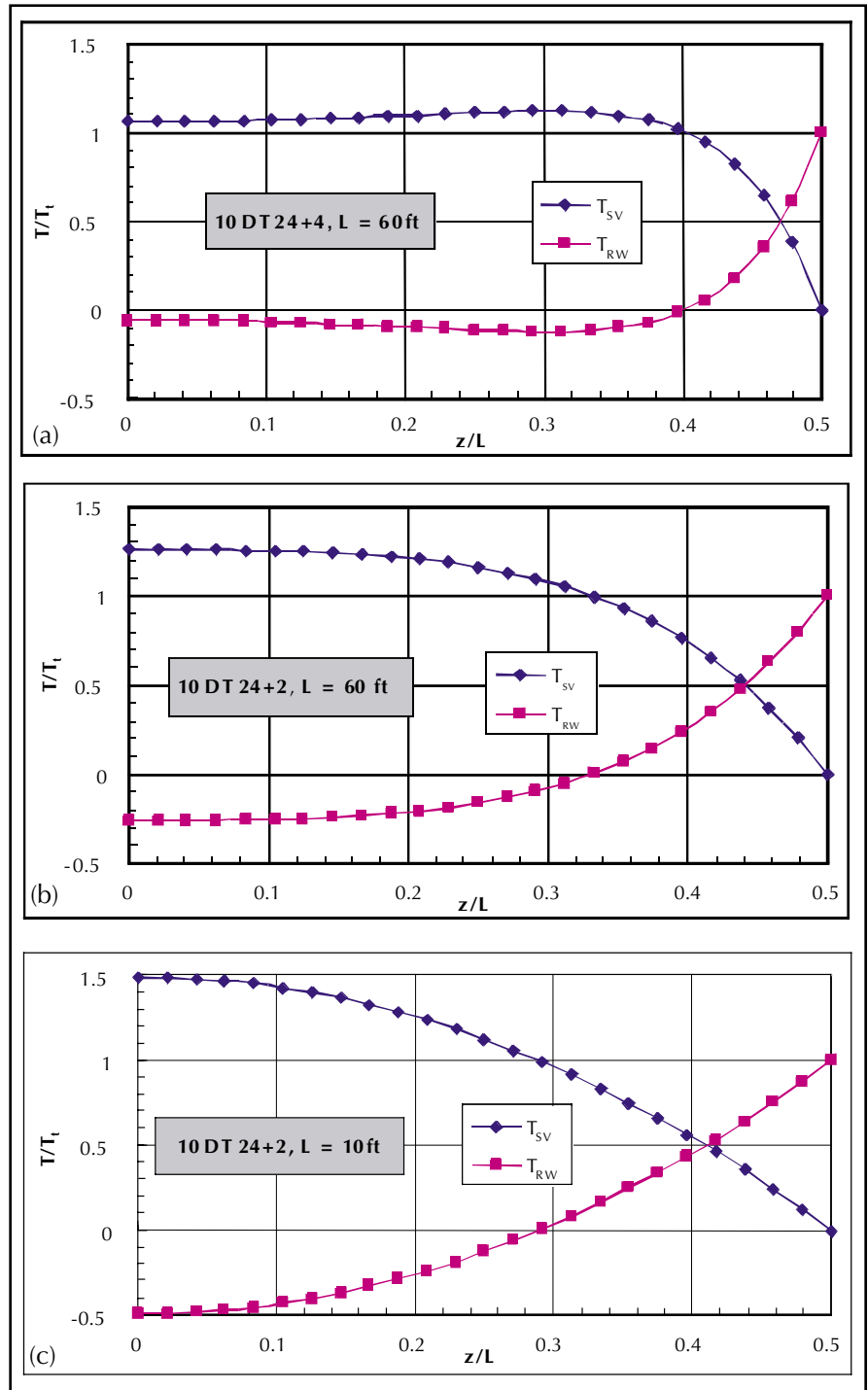

Fig. 8. Torque components versus span for three double tees: (a) 10DT24+4_60 (analytical model), (b) 10DT24+2_60 (analytical model), and (c) 10DT24+2_10 (analytical model).

of the members, as discussed below. Rigid supports were provided under three of the web ends, and a vertical load was applied at the fourth.

The shell elements were located at the centerlines of the webs and flange. The total height of the web elements was, therefore, the clear height of the web, 24 in. (610 mm), plus half the flange thickness. These same dimensions were used for computing the member properties in the analytical and FD solutions shown in Figs. 7 and 8, in order to facilitate comparisons. In the analytical and FD solutions, the torsional stiffness of the components, and in particular the webs, was taken as $bt^3/3$, rather than the more precise value that depends on the b/t ratio of the component, because that is the value used in the FE model.

Tests with different mesh sizes showed that the flange bending moment at a location close to the web-flange junction and 10 in. (250 mm) from the end of the member changed by less than 1 percent as the mesh size was reduced from 10 to 2.5 in. (250 to 62 mm). The data shown in the figures are for meshes with maximum element dimensions of 5 in. (127 mm) for the 60 ft (18.3 m) members and 2.5 in. (62 mm) for the 10 ft (3.05 m) member.

To compare the FE solution with the analytical and FD solutions, the twist angle due to rigid body rotation of the cross section, ϕ_r, was taken as the average of the rotations at the top and bottom of each web:

$$\phi_r = \frac{\phi_{TS} + \phi_{BS} + \phi_{TL} + \phi_{BL}}{4} \qquad (34)$$

where

ϕ_{TS} = rotation about longitudinal axis at top of supported web

ϕ_{BS} = rotation about longitudinal axis at bottom of supported web

ϕ_{TL} = rotation about longitudinal axis at top of loaded web

ϕ_{BL} = rotation about longitudinal axis at bottom of loaded web

The total twist angle, ϕ_t, was taken as the difference in vertical displacement between the centerlines of the webs, u_y, divided by the centerline distance, s, between the webs:

$$\phi_t = \frac{u_y}{s} \qquad (35)$$

where

u_y = difference in vertical displacement between two webs

s = centerline distance between webs of double tee

The twist angle due to distortion of the cross section was then taken as the difference between the total twist angle and that due to rigid body rotation:

$$\phi_d = \phi_t - \phi_r \qquad (36)$$

Figs. 7a to 7c show the twist angles computed using the FE model compared with the FD and analytical solutions; the FE solutions are shown as discrete symbols. The FE results are very close, but not identical, to the other two. The differences are smallest when the flange is the most flexible (10DT24+2_10) and largest for the stiff flange case of the 10DT24+4_60. The agreement suggests that the analytical

model captures the main trends in behavior, whereas the differences suggest that the primary shortcoming lies in the modeling of the stiffness of the flange between the webs.

Eq. (8), which defines the flange bending stiffness, ignores the coupling between the out-of-plane moments in the transverse and longitudinal directions, whereas it is included automatically in the FE computations. This is the most likely source of the error. However, the differences between the FE and analytical results, over a wide range of member properties, are much smaller than other potential sources of error, such as the modulus of rupture of the concrete, so the new model may be considered good enough for design purposes.

In addition to the twist angle, the flange bending moment is of practical interest. Because the flange bending moment is proportional to the second derivative of ϕ_r [as shown by Eqs. (8) and (10)], it is much more difficult to predict than ϕ_r itself; thus, it constitutes a severe test of the analytical model's fidelity. Fig. 9 shows the distribution of the flange bending moment as computed using the FE and analytical models for the same structures as were used in Figs. 7 and 8.

For each of the double tee structures, the flange moments predicted by the FEA follow the same general pattern as those predicted by the analytical model, peaking at the member end and decaying toward midspan. The agreement is best when the flange is flexible relative to the webs.

In all cases, the FE solution for the flange bending moment differs in two respects from the analytical model at the ends of the member.

First, in the end region, the FE model predicts slightly higher flange bending moments than does the analytical model. The exact reason for this difference is unknown, but it is assumed that it is because the FE solution includes modes of response that are not present in the analytical model.

Second, at the very end, the FE solution shows a sudden drop in flange moment.

It is worth noting that the CEG researchers appear to have found a similar behavior in their analyses.[3] The CEG report states: "Once the maximum stress is reached, it occurs initially over a length of 3 in. [76 mm]." The CEG researchers used a 1 in. (25 mm) mesh size.

This drop in flange bending moment predicted by the FE models arises because of the coupling between the longitudinal and transverse moments in the flange and the fact that the longitudinal flange moment must be zero at the free end. This fact was verified using a FE model for the member with a 2 in. (51 mm) flange in which Poisson's ratio was taken equal to zero (shown in Fig. 9 as $nu = 0$).

This decouples the longitudinal and transverse moments and eliminates the drop in flange moment at the end. These two tendencies partially counteract each other, so the peak moment predicted by the analytical method is only 3, 5, and 9 percent lower than that of the FEA for the three cases, respectively. (The 9 percent error occurs with the 10DT24+2_10, which is an improbable structure in practice.)

In addition to the mechanisms discussed above, the precise value of the peak flange bending moment is influenced slightly by out-of-plane shear stresses, as demonstrated by the fact that the thick- and thin-plate FE solutions gave slight-

ly different values. (The thick-plate values are not shown.) However, the discrepancy between the flange bending moments predicted by the FE and analytical solutions is smaller than uncertainties associated with the cross-section geometry that are discussed below, so it is proposed that no correction factor be used.

The good agreement between the analytical and FE solutions shows only that the analytical model can reproduce the results of the FE model, but this still presupposes that the FE solution represents accurately the true behavior of the member. Although that representation is expected to be close, several issues remain to be verified. Examples are the effects of tapered webs, the use of shell elements placed at the element centerlines rather than using explicit element thicknesses, the effect of fillets at the web-flange junction, and the neglect of the shear deformations of the web and flanges. The consequences of these modeling assumptions can best be determined by physical testing.

PARAMETERS INFLUENCING FLANGE BENDING STRESS

In this section, the effects on the flange bending stress of varying the primary parameters are studied. The new torsional model is used because it offers the simplest way of conducting the calculations, and because the foregoing sections demonstrate that it closely represents the behavior of the system.

Further consideration is given to the calculation of the geometric parameters used in the analytical model to ensure that the true geometry of the double-tee member is modeled as accurately as possible. Plots are provided showing the impact of span length, flange width and thickness, and web depth and thickness on flange bending moment.

Calculation of Section Properties

In validating the analytical model through comparison with the FE model, the cross-sectional properties were computed using a "line model," in which all the material was treated as being concentrated along the centerlines of the webs and flanges. This model provided the closest approximation to the FE model, which was constructed using shell elements that have no explicit manifestation of thickness. This approach, however, leads to a somewhat imperfect description of the sections that are used in practice. To rectify this situation, several enhancements were made to the analytical model to enable a closer representation of real double-tee cross sections.

First, the true geometry of the double tee was considered in calculating the St. Venant torsional constants, J, for the webs and flanges. To account for the aspect ratio of the webs and flanges, com-

ponent torsional constants were computed using the following empirical equation:

$$J = \frac{bt^3}{3}\left\{1 - 0.630\frac{t}{b}\left[1 - \frac{1}{12}\left(\frac{t}{b}\right)^4\right]\right\} \qquad (37)$$

where t is the average thickness (smaller dimension) of the component (web or flange) and b is the average width (larger dimension) of the component.

This equation was developed by fitting a curve to discrete results that were obtained numerically. It accounts approximately (with an error of less than 1 percent) for the variation in J with t/b. The effects of web and flange taper were accounted for by multiplying J by the approximate factor c_J:

$$c_J = 1 + \left(\frac{t_{w,top} - t_{w,bot}}{t_{w,top} + t_{w,bot}}\right)^2 \qquad (38)$$

The true effect of a tapered web on J depends on both the aspect ratio of the web and the degree of taper; however, no single equation exists that addresses both factors. Use of Prandtl's soap film analogy shows that Eq. (38) gives the exact correction for components with $t/b = 0$. In the interest of simplicity, it was used in the current study.

In addition to considering the geometry of the webs and flanges individually, the finite dimension of the web-flange intersections also was incorporated into the model. This was done in three ways.

First, to account for the impact of the web-flange intersection on the cross section shear stiffness, the torsion constant of the web, J_w, was increased using the approach suggested by Mack et al.[1] This consists of taking for the effective web height the clear height below the flange plus a multiple, n_{tf}, of the flange thickness. Mack et al. found that the value $n_{tf} = 2.0$
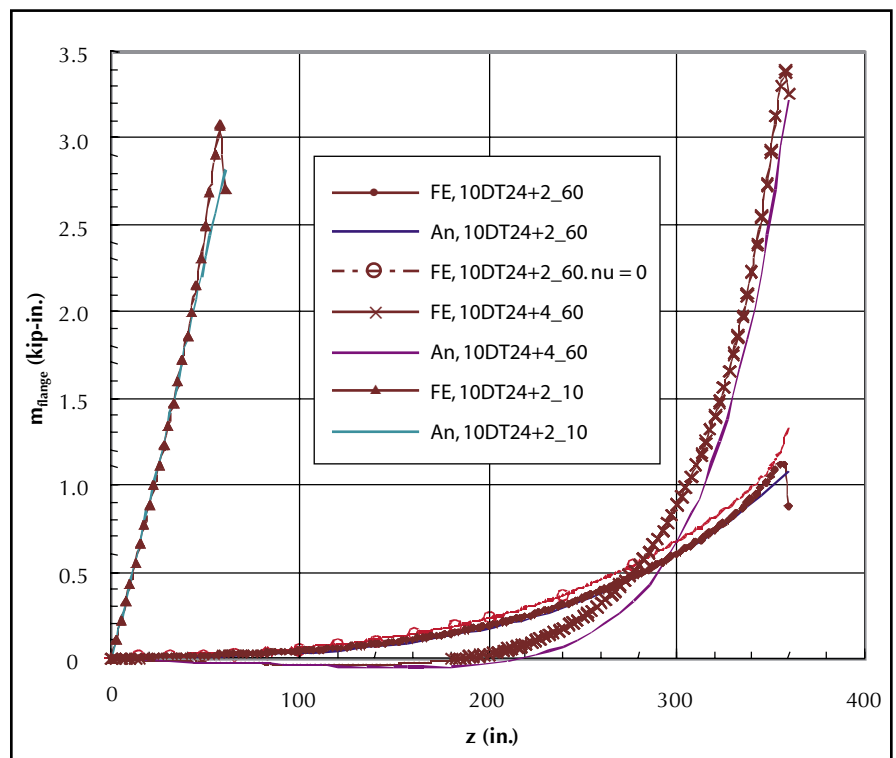

Fig. 9. Peak flange bending moment versus location (all sections—finite element analysis and analytical method).

gave *J* values closest to those provided by a Prandtl soap film analysis, so that value was used here.

Second, to account for the impact of the web-flange intersection on the distortional stiffness of the flange, the flange was treated as having a rigid-end offset. The parameter REO_k is used to define the relative increase in stiffness associated with the rigid offset. Specifically, REO_k is defined as the length of the rigid offset at each web, normalized with respect to the half-width of the web.

Setting $REO_k = 1.25$ indicates that the flange is treated as rigid for a distance from the web centerline equal to 1.25 times the half-width of the top of the web. Use of REO_k greater than zero stiffens the flange by reducing the length over which it is free to bend. An REO_k value greater than 1.0 implies the existence of a fillet at the web-flange junction.

The parameter REO_k is incorporated into the analysis by replacing D_f by $D_{f,eff}$, where:

$$D_{f,eff} = \frac{D_f}{(1 - \zeta_k)^3} \qquad (39)$$

and

$$\zeta_k = \frac{REO_k t_{w,top}}{s} \qquad (40)$$

The parameter $D_{f,eff}$ is used both in computing ν in Eq. (15) and for computing $m_{f,max}$ in Eq. (28).

Third, to improve the calculation of the maximum flange bending stress, the flange moment was evaluated at a location away from the intersection of the web and flange centerlines. This distance is referred to as REO_m and is defined in the same way as REO_k. Use of REO_m greater than zero reduces the value of the computed moment. The parameter REO_m is incorporated into the analysis by multiplying the maximum flange moment, $m_{f,max}$, computed from Eq. (28) by $(1 - \zeta_m)$ where:

$$\zeta_m = \frac{REO_m t_{w,top}}{s} \qquad (41)$$

Both REO_k and REO_m can be specified independently; however, the two parameters are likely to have very similar values.

The modifications to the basic model can be summarized as a vector of modification constants:

$$Modcon = (REO_k, REO_m, n_{tf}, \text{taper factor}, J \text{ factor}) \qquad (42)$$

The taper factor and *J* factor are triggers with values 0 or 1 to invoke the use of the basic or refined value. For comparison with the analytical and FE solutions (data shown in Figs. 7 and 8), the basic *Modcon* values (0, 0, 0.5, 0, 0) were used. However, in evaluating the impact of member geometry on flange stress, the following refined values were used: (1.25, 1.25, 2.0, 1, 1). These values are believed to represent as best possible the true properties of a typical double tee.

Flange Bending Stresses

To investigate the impact of double tee geometry on flange bending stress, the refined analytical model was used to model a range of double tees. Fig. 10 shows normalized flange bending stresses for the double tees analyzed.

The double tees included in the analyses had member spans ranging from 10 to 70 ft (3.05 to 21.3 m) and member depths ranging from 18 to 36 in. (457 to 914 mm). In all cases, the flange thickness was defined to be 2 in. (51 mm), the web was assumed to vary in thickness from 5 in. at the bottom to 8 in. at the top (125 to 200 mm), with the average web thickness defined to be 6.5 in. (165 mm), and *Modcon* = (1.25, 1.25, 2.0, 1, 1).

Following the assumptions used to develop the new torsion model, the flange bending stress is given by:

$$\sigma_f = \frac{6m_{f,max}}{t_f^2} \qquad (43)$$
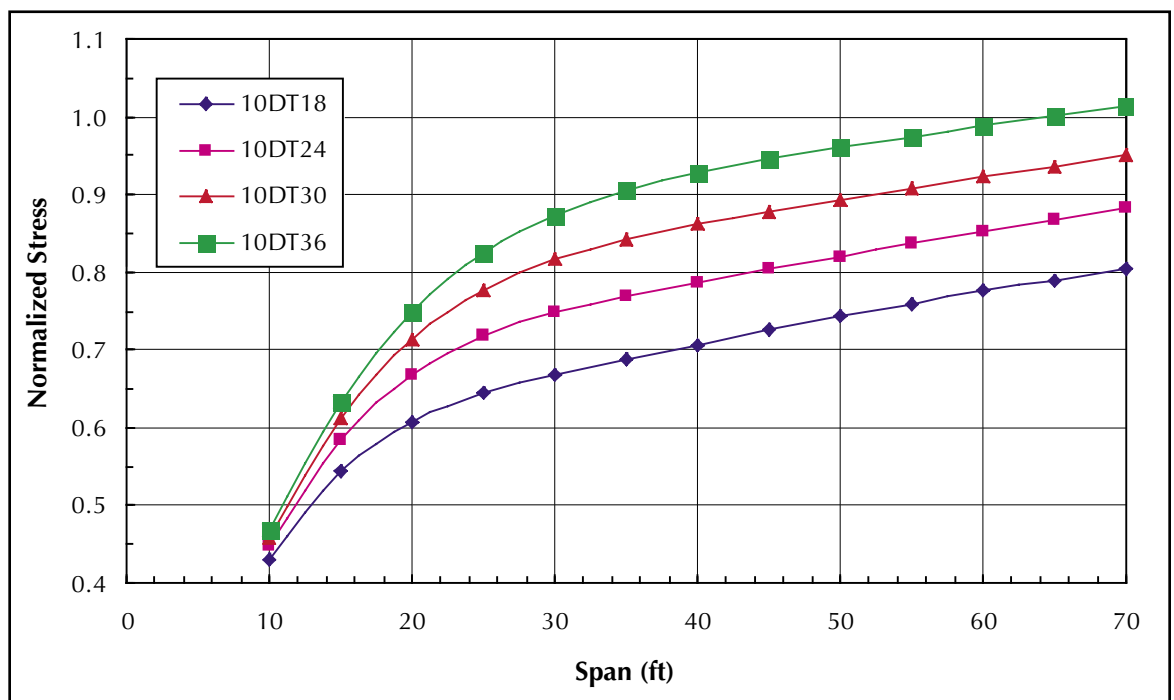

Fig. 10. Normalized flange bending stress versus span length.

where $m_{f,max}$ is the maximum flange bending moment [Eq. (28)] observed along the length of the member.

Note that the analytical model predicts that the maximum stress occurs at the end of the member.

Concrete cracking is of primary importance in the design of double tees. ACI 318-02[9] defines concrete cracking stress as a multiple of $\sqrt{f_c'}$, so it is convenient to normalize the bending stress by dividing it by $\sqrt{f_c'}$. The maximum flange moment, $m_{f,max}$, is a function of the concrete elastic modulus, E, which also is defined typically as a function of $\sqrt{f_c'}$.

Thus, the maximum normalized concrete tensile stress is independent of the concrete compressive strength, and concrete material properties need no longer be considered in the calculations. (Note that Poisson's ratio, ν_c, does have a small effect on the stress calculations but is taken to be 0.20 throughout.)

To facilitate the use of the data presented in Fig. 10, concrete stress is presented normalized with respect to $\sqrt{f_c'}$ and with respect to the average twist per unit length [$(\phi_0/L) \times 10^6$]. Thus, the ordinate, c_σ, in Fig. 10 is defined by:

$$c_\sigma = \frac{\sigma_f}{\sqrt{f_c'}} \frac{L}{\phi_0 \times 10^6} \qquad (44)$$

where L is measured in inches and ϕ_0 in radians.

Thus, for a member with $L = 720$ in. subjected to a total twist of $\phi_0 = 0.012$ radians, a normalized stress ordinate of $c_\sigma = 0.6$ corresponds to a stress of $10\sqrt{f_c'}$ (psi) [$0.830\sqrt{f_c'}$ (MPa)]. This is computed as follows:

$$\sigma_f = c_\sigma \frac{\phi_0 \times 10^6}{L} \sqrt{f_c'}$$

$$= 0.6 \frac{(0.012 \times 10^6)}{720} \sqrt{f_c'}$$

$$= 10\sqrt{f_c'} \text{ (psi)} \left[0.830\sqrt{f_c'} \text{ (MPa)} \right] \qquad (45)$$

The data in Fig. 10 show that for a given section and twist angle, the induced torque (and thus flange moment) is not directly proportional to the member length. This is so because the total twist angle consists of ϕ_d, which dominates at the member ends, and ϕ_r, which dominates in the body of the member.

As the member length changes, the relative contributions of the two components differ. A long member has about the same amount of "end" but more "middle" than does a shorter one, so the overall torsional stiffness is a nonlinear function of the span length.

Figs. 11a to 11e show the impact on flange bending stress of variations in member length, flange thickness, web spacing, web depth, and web thickness. In all cases, the reference value is for a 10DT24+2_60 with REO values of 1.25 and is obtained from Fig. 10. The vertical ordinate in Figs. 11a to 11e gives the factor by which the stress must be multiplied if the normalized stress is read from the 10DT24+2 curve in Fig. 10. In each of Figs. 11a to 11e, only one characteristic is changed so that its individual influence can be seen.

Figs. 11a and 11b show the impact of member length and flange thickness on bending stress. Fig. 11a shows how the impact of flange thickness varies with member length, while Fig. 11b provides data for three specific member lengths. The data in Figs. 11a and 11b show that the 2 in. (51 mm) flange thickness leads to the highest bending stress at all spans except very short ones [i.e., less than about 15 ft (4.5 m)].

The flange thickness affects both the demand and the capacity. A thinner flange leads to more cross-section distortion and lower induced flange bending moments for a given twist angle. However, the section modulus of the flange and, thus, its cracking moment are also smaller. The data from Figs. 11a and 11b show that, for most practical spans, the stiffness effect dominates and the thinner flange is the more vulnerable.
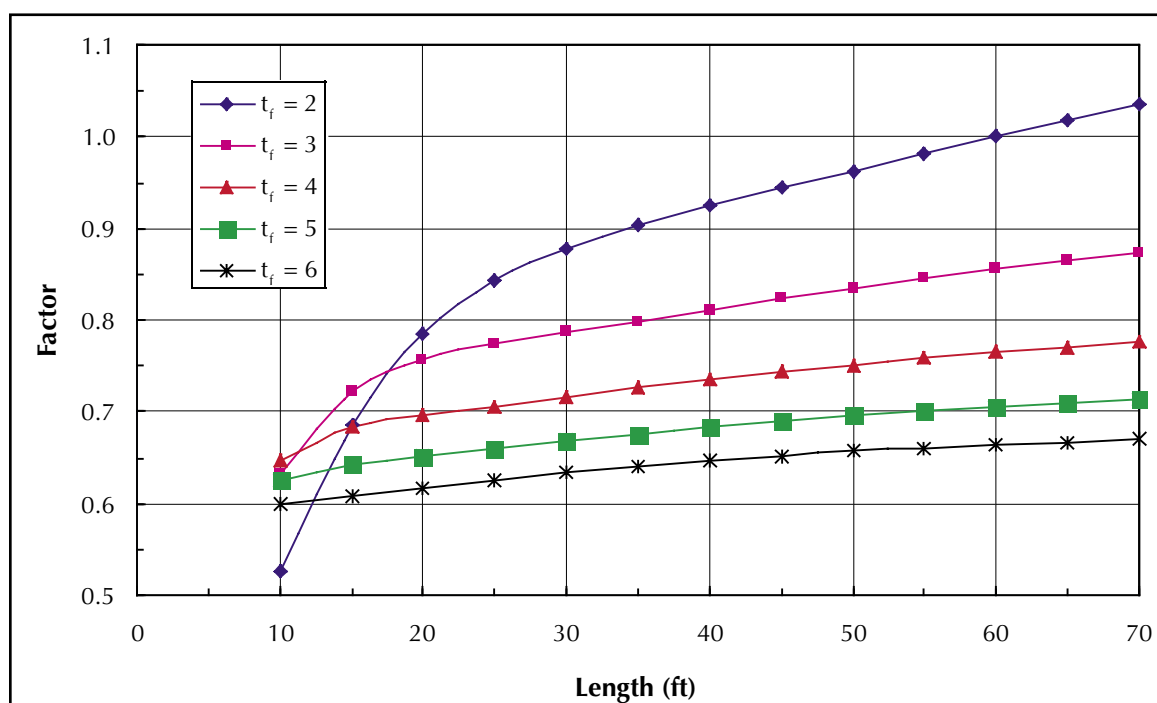

Fig. 11a. Stress correction factor for length.

Fig. 11c shows the impact of web spacing on flange stress. The data in this figure show that for all member lengths, a greater web spacing leads to a lower stress for a given total twist angle. As with the flange thickness, this result is the consequence of two opposing effects. A larger web spacing reduces the flange moment for a given distortion rotation, ϕ_d, but it also makes the flange more flexible; thus, ϕ_d is a higher proportion of the total twist angle. The first effect is stronger than the second, and the net result is a reduction in flange moment (and stress) with an increase in web spacing.

Figs. 11d and 11e show the impact of web depth and thickness on flange moment and bending stress. The data in Fig.

11d indicate that increased web depth results in increased bending stress. This can be attributed to increased deformation due to cross-section distortion and, thus, increased flange bending moment. The data in Fig. 11e show that flange stress increases as web thickness increases, which can be attributed to the fact that increased web thickness results in increased cross-section distortion and, thus, increased flange moment and stress.

Review of the data in Figs. 11a to 11e shows that, over the range of dimensions commonly used in practice, web thickness and web spacing exert the strongest influence on response. Flange thickness plays a relatively minor role.
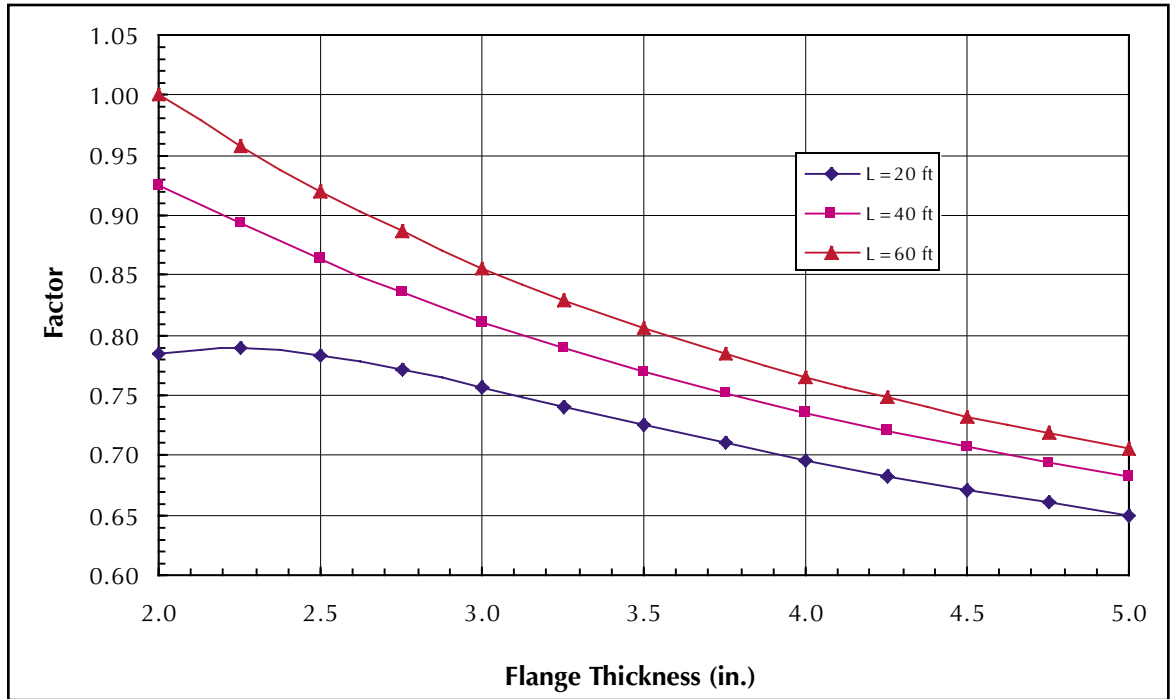

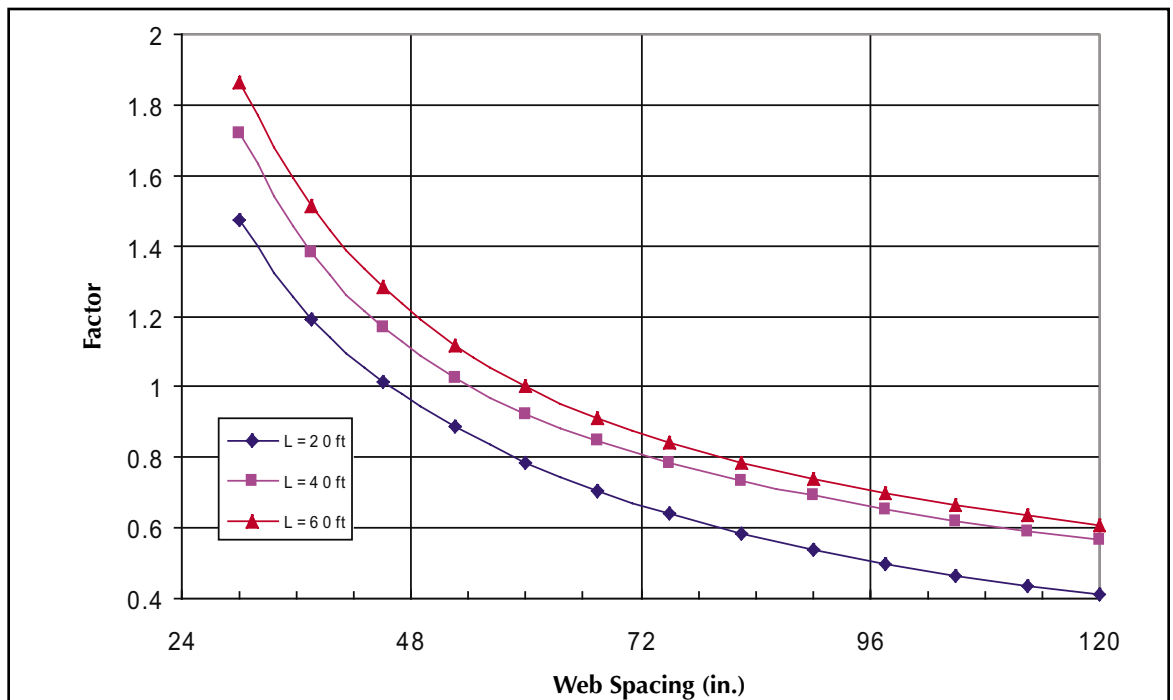Fig. 11b. Stress correction factor for flange thickness.

Fig. 11c. Stress correction factor for web spacing.

54

APPLICATION OF THE MODEL TO COMPUTE FLANGE STRESS

The peak flange bending stress depends on the member properties and the twist angle to which the double tee is subjected. Two methods for computing the stress are presented here.

The first method makes direct use of the equations developed using the new torsional model. This method is the more general approach and can be applied to any section size or shape. The primary disadvantage is the amount of calculation needed, although this can be ameliorated by programming the equations into a spreadsheet, as was done for this study.

The second method makes use of the data provided in Figs. 10 and 11. This method still requires the calculation of the section properties, particularly the values of J and C_w, but requires less computational effort thereafter. Parameters J and C_w cannot readily be standardized because they are relatively sensitive to the web thickness, which, for any given tee depth, differs among manufacturers. Each method is demonstrated by means of an example.

Method A: Direct Calculation

The previously developed equations are used to compute the maximum flange bending moment and bending stresses
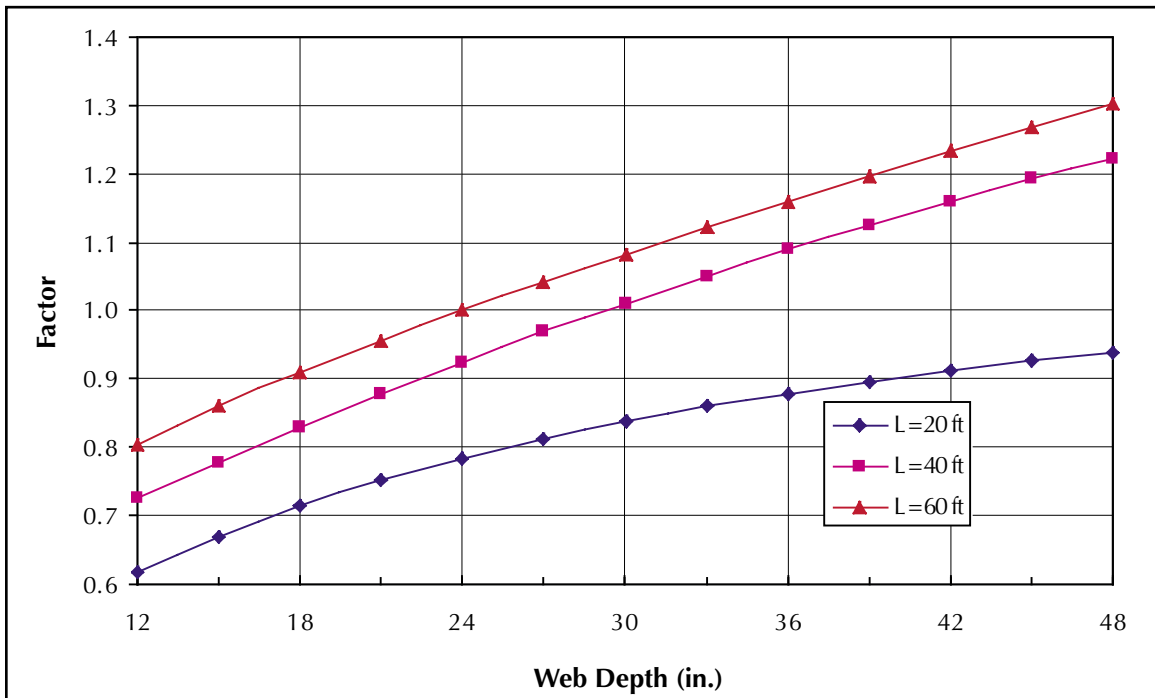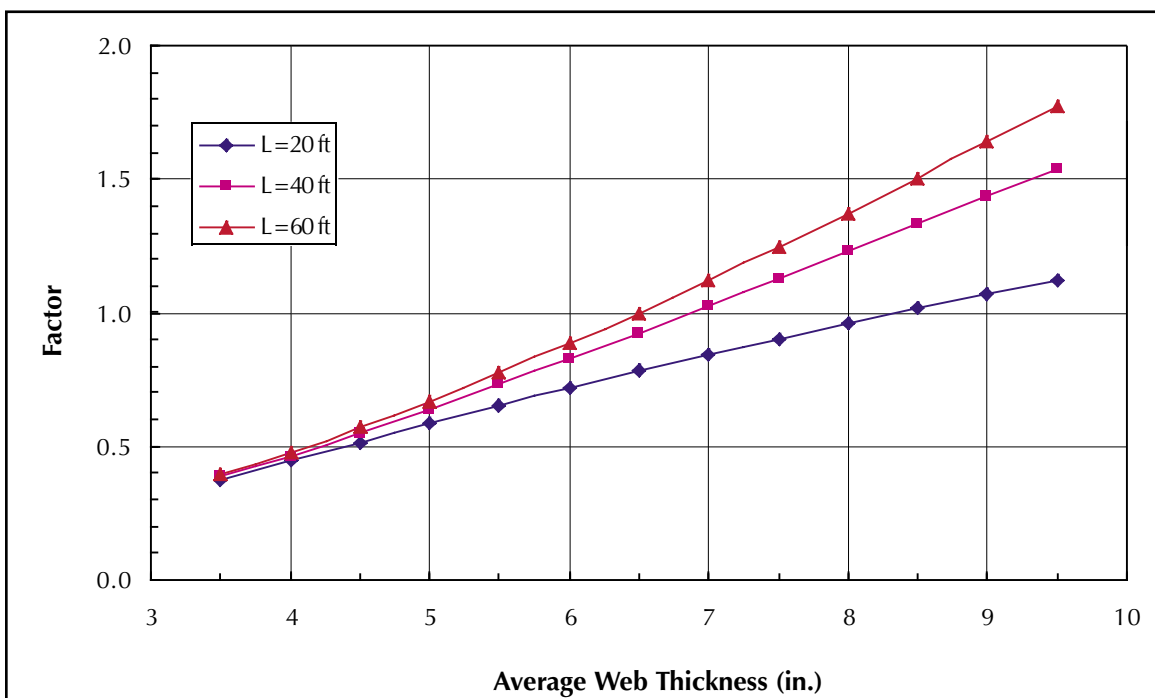

Fig. 11d. Stress correction factor for web depth.

Fig. 11e. Stress correction factor for average web thickness.

for a double tee with standard dimensions subjected to a pre-determined twist angle.

Example double tee—Consider a 10DT24+4 spanning 60 ft (18.3 m) for which one stem end is seated 0.75 in. (19 mm) lower than the other three. The cross-sectional dimensions are given in Table 1. It is assumed that corner fillets render the flange rigid for 1 in. (25 mm) beyond the face of the web, for calculation of both stiffness and flange moment.

Calculation of required material properties—The concrete is assumed to have $f'_c = 6000$ psi (41 MPa) and $\nu_c = 0.2$, from which:

$$E_c = 57\sqrt{f'_c} = 57\sqrt{6000}$$
$$= 4415 \text{ ksi (30.44 GPa)}$$

$$G_c = E_c/2(1 + \nu_c) = 4415/2(1 + 0.2)$$
$$= 1839.7 \text{ ksi (12.69 GPa)}$$

Calculation of required section properties—The St. Venant torsion properties are computed first using the refined modeling approach that accounts for the web taper. For the flange:

$$t_f/b_f = 4/120 = 0.01333$$

$$J_f = \frac{bt^3}{3}\left\{1 - 0.630\,\frac{t}{b}\left[1 - \frac{1}{12}\left(\frac{t}{b}\right)^4\right]\right\}$$

$$= 0.3263bt^3 = 2506 \text{ in.}^4 \ (1.043 \times 10^9 \text{ mm}^4)$$

For each web:

$$h_{eff} = h_w + n_{tf}(t_f) = 24 + 2(4) = 32 \text{ in. (813 mm)}$$

$$t_{w,ave} = 0.5(5 + 8) = 6.5 \text{ in. (165 mm)}$$

$$t/b = t_{w,ave}/h_{eff} = 6.5/32 = 0.2031$$

The taper factor, c_J, computed using Eq. (38), is:

$$c_J = 1 + \left(\frac{t_{w,top} - t_{w,bot}}{t_{w,top} + t_{w,bot}}\right)^2 = 1 + \left(\frac{8-5}{8+5}\right)^2 = 1.0533$$

$$J_w = c_J\,\frac{bt^3}{3}\left\{1 - 0.630\,\frac{t}{b}\left[1 - \frac{1}{12}\left(\frac{t}{b}\right)^4\right]\right\}$$

$$= 1.0533 \times 0.2907bt^3 = 2691 \text{ in.}^4 \ (1.120 \times 10^9 \text{ mm}^4)$$

$$J = J_f + 2J_w = 7887 \text{ in.}^4 \ (3.283 \times 10^9 \text{ mm}^4)$$

$$GJ = 1839.7(7887) = 14.51 \times 10^6 \text{ kip-in.}^2 \ (41640 \text{ kN-m}^2)$$

To compute the restraint-of-warping torsion constant, C_w, the taper in the webs is ignored and, in the interest of simplicity, the member is treated as thin-walled. Thus, the properties can be obtained from standard texts on mechanics of materials.[2] The web height for calculating C_w is the centerline

dimension, which is given by the clear height plus half the flange thickness, or 26 in. (661 mm) in this case.

The vertical eccentricity of the shear center, e_{SC}, is:

$$e_{SC} = h_w\Big/\left(2 + \frac{b_f^3 t_f}{3s^2 h_w t_w}\right)$$

$$= h_w\Big/\left[2 + \frac{(120^3)(4)}{(3)(60^2)(26)(6.5)}\right]$$

$$= 0.1728h_w = 4.493 \text{ in. (114 mm)}$$

Computation for C_w is then:

$$C_w = t_w h_w^2 s^2(2h_w - 3e_{SC})/12$$

$$= 6.5(26^2)(60^2)[2(26) - 3(4.493)]/12$$

$$= 50.78 \times 10^6 \text{ in.}^6 \ (13.64 \times 10^9 \text{ mm}^6)$$

$$EC_w = 4415(50.78 \times 10^6)$$

$$= 224.2 \times 10^9 \text{ in.}^4\text{-kips (1.851 kN-m}^4)$$

The flange bending stiffness is:

$$D_f = \frac{Et_f^3}{12(1 - \nu_c^2)} = \frac{4415 \times 4^3}{12(1 - 0.2^2)}$$

$$= 24,530 \text{ in.}^2\text{-kip/in. width (2.771 kN-m/m width)}$$

Calculation of rigid end offset parameters—The impact of the finite-volume web-flange joint is modeled as follows:

$$REO_k = \frac{2 + t_{w,top}}{t_{w,top}} = \frac{2+8}{8} = 1.25$$

$$\zeta_k = \frac{REO_k t_{w,top}}{s} = \frac{1.25 \times 8}{60} = 0.1667$$

$$c_k = \left(\frac{1}{1 - \zeta_k}\right)^3 = \left(\frac{1}{1 - 0.1667}\right)^3 = 1.728$$

$$D_{f,eff} = c_k D_f = (1.728)(24,530)$$

$$= 42,390 \text{ in.}^2\text{-kips/in. width (4.789 kN-m/m width)}$$

To allow for the rigid end offset in calculating the moment:

$$\zeta_m = \frac{REO_m t_{w,top}}{s} = \frac{1.25 \times 8}{60} = 0.1667$$

$$c_m = \frac{1}{1 - \zeta_m} = \frac{1}{1 - 0.1667} = 1.2$$

Dimensionless parameters:

$$\lambda L = L\sqrt{\frac{GJ}{EC_w}} = 720\sqrt{\frac{14.51 \times 10^6}{224.2 \times 10^9}}$$

$$= 720 \times 0.008045 = 5.792$$

$$vL = L\sqrt{\frac{3D_{f,eff}}{sGJ_w}} = 720\sqrt{\frac{3 \times 42,390}{60 \times 4.950 \times 10^6}}$$

$$= 720 \times 0.02069 = 14.90$$

From Fig. 6 [or Eqs. (18) to (21)]:

$$c_t = 8.445$$

Calculation of maximum flange moment and bending stress—The total twist angle is computed as follows:

$$\phi_0 = \frac{\Delta}{s} = \frac{0.75}{60} = 0.0125 \text{ rad}$$

From the total twist angle, the twist angle due to distortion is computed using Eq. (17b):

$$\phi_d\left(\frac{L}{2}\right) = \left(\frac{\phi_0/2}{1+c_t}\right) = \left(\frac{0.0125/2}{1+8.445}\right) = 0.667 \times 10^{-3} \text{ rad}$$

The peak flange moment is computed using Eq. (28) and the modification factors $D_{f,eff}$ and c_m defined by REO_k and REO_m:

$$m_{f,max} = \frac{6D_{f,eff}}{c_m s}\phi_d\left(\frac{L}{2}\right) = \frac{6 \times 42,390}{1.2 \times 60}\, 0.0006617$$

$$= 2.337 \text{ kip-in./in. width (10.39 kN-m/m width)}$$

The maximum flange bending stress is computed using Eq. (43) as:

$$\sigma_f = \frac{6m_{f,max}}{t_f^2} = \frac{6 \times 2.337}{4^2} = 876.5 \text{ psi}$$

$$= 11.32\sqrt{f_c'} \text{ (psi) } [0.939\sqrt{f_c'} \text{ (MPa)}]$$

Consideration of self-weight and the applied torque—It may be of interest to determine whether the member will twist enough under its own weight to rest on the four supports. The torque applied due to self-weight is given by:

$$T_t = \frac{W}{2}\frac{s}{2} = \frac{49.5 \times 60}{4} = 742.5 \text{ in.-kips (83.89 kN-m)}$$

The twist angle due to self-weight of the member can then be obtained using Eqs. (6) and (27) as:

$$\phi_0 = \frac{T_tL}{GJ}\left(1 + \frac{1}{c_t}\right) = \frac{742.5 \times 720}{14.51 \times 10^6}\left(1 + \frac{1}{8.445}\right)$$

$$= 0.04121 \text{ rad}$$

This value is significantly larger than the difference in slope between the two supports of 0.0125 radians, so the member will rest on the supports under its own weight.

Method B: Calculation Using Design Charts

In the direct method outlined above, the calculations are quite extensive and involve variables that are not commonly used in concrete construction. Thus, an alternative approach is presented in this section that obviates the need for many of the calculations shown above. This approach uses the data provided in Figs. 10 and 11 as design charts. The penalty for

using this approach is a slight loss of accuracy that is inevitable when interpolating between curves on graphs.

Normalized flange bending stresses are presented in Fig. 10 for several representative double-tee sizes, spanning a range of distances that center on those used in practice, particularly the 55 to 65 ft (17 to 20 m) span that is used commonly in parking structures. In the interest of standardization, the web thicknesses are all the same [8 in. (200 mm) top and 5 in. (125 mm) bottom], and the refinements described above (web taper, rigid end offset, and so on) were used in all cases.

The effect of slight variations from these standard dimensions can be estimated by the information in Figs. 11a to 11e. The data in Figs. 10 and 11 are used as follows:

Example double tee—Consider the same member as in the last example, namely, a 10DT24+4 spanning 60 ft (18.3 m). To achieve drainage, one of the four supports is to be lowered by 0.75 in. (19 mm) with respect to the plane defined by the other three.

Calculation of average twist—The average twist per unit length of the double tee is:

$$\frac{d\phi}{dz} = \frac{\Delta}{sL} = \frac{0.75}{60 \times 720}$$

$$= 17.36 \times 10^{-6} \text{ rad/in. } (0.6835 \times 10^{-3} \text{ rad/m})$$

Calculation of maximum bending stress using Figs. 10 and 11—The ordinate in Fig. 10 for a 10DT24+2 gives the stress divided by $\sqrt{f_c'}$ per average rate of twist as 0.855. This value must be corrected for flange thickness. Fig. 11b gives a correction factor of 0.763 for a 60 ft (18.3 m) span and a 4 in. (100 mm) thick flange. Thus, the maximum flange bending stress can then be obtained as a multiple of $\sqrt{f_c'}$ as:

$$\sigma_f = 0.855 \times 0.763 \times \sqrt{f_c'} \times \frac{d\phi}{dz} \times 10^6$$

$$= 0.652 \times \sqrt{f_c'} \times 17.36 \times 10^{-6} \times 10^6$$

$$= 11.3\sqrt{f_c'} \text{ (psi) } [0.904\sqrt{f_c'} \text{ (MPa)}]$$

For $f_c' = 6000$ psi (41.4 MPa), the absolute stress is:

$$\sigma = 11.3\sqrt{f_c'} = 11.3\sqrt{6000} = 875 \text{ psi (7.10 MPa)}$$

This result is almost identical to the 876.5 psi (6.04 MPa) computed using the exact equations. Note that the graphs present the stress in dimensionless form (i.e., stress divided by $\sqrt{f_c'}$), regardless of the value of E used. This is possible if E is taken to be $57,000\sqrt{f_c'}$ (psi). If E is known to have some other value, the stress must be scaled accordingly.

Evaluation of results—The 60.5 ft (18.4 m) long double tee tested by CEG had the foregoing cross-sectional dimensions and cracked at a vertical web displacement between 0.6875 and 0.75 in. (17.5 and 19.0 mm). If the average of these two values [0.7188 in. (18.2 mm)] is used, and the member is assumed to span 60 ft (18.3 m) between support centers, the computed bending stress is $10.8\sqrt{f_c'}$, or 840 psi if $f_c' = 6000$ psi ($0.858\sqrt{f_c'}$, or 5.79 MPa if $f_c' = 41.4$ MPa).

This value lies within the range of modulus of rupture values commonly observed in laboratory tests. It would obvi-

ously be slightly different if other assumptions were made about the magnitude of the rigid end offsets. This value was obtained using top and bottom web thicknesses of 8 and 5 in. (200 and 125 mm).

Mack et al.[1] imply that the double tee tested by CEG[3] had web thicknesses of 7.75 and 4.75 in. (197 and 121 mm) in accordance with the *PCI Design Handbook*.[10] The predicted flange bending stress would then change to $10.2\sqrt{f'_c}$ psi ($0.846\sqrt{f'_c}$ MPa).

Using the refined approach presented in this paper, the St. Venant torsion constant, J, for this member is computed as 7887 in.[4] (3.283×10^9 mm^4). Given this value, the method proposed by Mack et al.[1] (their Fig. 11) predicts a shear stress of 375 psi for a 2 in. (2.59 MPa for a 51 mm) warp deflection, measured between the flange tips. This may be scaled linearly to 270 psi, or $3.49\sqrt{f'_c}$, for 0.7188 in. warp measured between the stems of the tee (1.86 MPa, or $0.289\sqrt{f'_c}$, for 18.26 mm warp).

SUMMARY AND CONCLUSIONS

When double tees are twisted through sufficiently large angles, they develop longitudinal cracks at the web-flange junction. The cracks are attributed to transverse bending of the flanges, which is not accounted for in classical torsion theory. A modification to classical torsion theory was developed to account for distortion of the cross section by flange bending, and it allowed the flange bending stresses to be predicted.

The equations of the modified theory were solved using both analytical and finite difference approaches, which were found to give essentially identical results. The analytical solution also was verified for representative geometries using finite element analysis.

The modified theory was used to predict peak flange bending stresses in example double tees, and the results were found to be in plausible agreement with the initiation of cracking in two field specimens tested by others. Insufficient field data were available to make a precise comparison.

Based on the results of this study, the following conclusions can be drawn:

1. The flange cracking at the ends of twisted double tees appears to be caused by flange bending stresses, and not by St. Venant torsional shear stresses. Flange bending causes transverse stresses at the web-flange junction that lead to tension on the top of the flange on one side and on the bottom on the other. These tension stresses are consistent with the longitudinal cracks at those locations seen in practice.

2. The modified torsion theory presented here can predict flange bending stresses that are qualitatively consistent with those found in the FE analyses and with the flange cracking observed in field tests by others. The value of the peak tension stress that the modified theory predicts is consistent with the twist angle at which cracking occurred in the field tests conducted by The Consulting Engineers Group.[3]

3. The flange bending causes the member's torsional stiffness to be lower than the value predicted using the classical St. Venant theory.

4. This analysis deals only with linearly elastic uncracked members. Propagation of cracks after initiation must be analyzed by other means.

5. The flange bending is largest at the end of the member, and it attenuates with increasing distance from the end.

6. Web thickness exerts the largest influence on the flange bending stress for a given rate of twist. Members with larger average web thicknesses develop larger flange bending stresses.

7. The web spacing also has a significant influence on the flange bending stresses. As web spacing increases, flange flexibility increases and flange bending stresses decrease.

8. The member depth and flange thickness have only moderate effects on flange bending stresses.

9. The flange moment drops slightly at the very end of the member, so the peak moment occurs at a short distance from the end. This behavior was not predicted by the new method, but it was apparent in the FE analyses. It was shown to be associated with the coupling of the flange moments in the two orthogonal directions. For members of practical dimensions, the peak moment predicted by the new method occurs within 6 percent of the value obtained by FE analysis.

RECOMMENDATIONS

After verification by laboratory testing, the method presented here may be used by engineers and producers to predict the onset of flange cracking at the ends of twisted double tees.

For further research, the following recommendations are made:

1. The foregoing stresses were predicted on the basis of a rational theory alone. Confirmation of the results by controlled laboratory testing is highly desirable.

2. The effects on the predicted flange stress of certain features of the cross-section geometry should be explored in greater detail. Examples are corner fillets, tapered webs, and treatment of the web-flange junction region in computing the torsion constant, J.

3. A more detailed investigation of the local drop in flange bending moment near the end of the member should be undertaken.

REFERENCES

1. Mack, P., Force, G., Magnesio, C., and Bryan, K., "The Practice of Warping Double Tees," PCI JOURNAL, V. 48, No. 1, January-February 2003, pp. 32-48.
2. Timoshenko, S. P., *Strength of Materials, Part II*, Van Nostrand Reinhold, New York, NY, 1958, 572 pp.
3. PCI Research and Development Committee, "Durability of Precast Prestressed Concrete Structures," Report prepared by The Consulting Engineers Group, Inc., San Antonio, TX, for the Precast/Prestressed Concrete Institute, Chicago, IL, 1995.
4. Barre de St. Venant, P.A. J-C., *Memoire des Savants Etrangers*, V. 14, 1855.
5. Banks, G. A., Lowes, L. N., and Stanton, J. F., "End Effects in Members Subjected to Torsion," Report No. SGEM 2004-01, Department of Civil and Environmental Engineering, University of Washington, Seattle, WA, 2004.
6. MATLAB, http://www.mathworks.com.

7. Hetenyi, M., *Beams on Elastic Foundation*, University of Michigan Press, Ann Arbor, MI, 1946, 255 pp.
8. SAP2000, Computers and Structures, Inc., Berkeley, CA, 2004.
9. ACI Committee 318, "Building Code Requirements for Structural Concrete (ACI 318-02) and Commentary (ACI 318R-02)," American Concrete Institute, Farmington Hills, MI, 2002.
10. *PCI Design Handbook: Precast and Prestressed Concrete*, Fifth Edition, Precast/Prestressed Concrete Institute, Chicago, IL, 1999.

APPENDIX – NOTATION

A = coefficient matrix in finite difference solution

b = width (i.e., larger dimension) of cross-section component

b_f = flange width

B = bi-moment

c_J = coefficient for torsional stiffness of tapered web

c_k = constant associated with rigid end offset for stiffness

c_m = constant associated with rigid end offset for moment

c_t = dimensionless constant that controls amplitude of distortion twist angle = c_η/ϱ

c_η = dimensionless constant defined in Eq. (19)

c_σ = ordinate of Fig. 10 equal to normalized stress defined by Eq. (44)

C_d = section distortion torsion constant

C_w = restraint-of-warping torsion constant

D_f = stiffness of flange per unit length of double tee

$D_{f,eff}$ = effective stiffness of flange per unit length of double tee

e_{SC} = vertical coordinate of shear center

E = Young's modulus of elasticity

G = shear modulus

h = distance between nodes in finite difference solution

h_{eff} = effective height of web, used to compute J for the web

h_w = height of web, measured to mid-thickness of flange

i = $\sqrt{-1}$ (imaginary number)

J = St. Venant torsion constant

J_f = St. Venant torsion constant for flange

J_w = St. Venant torsion constant of one web

$K_{\theta,end}$ = stiffness of torsional spring in series with member

L = span length

m_f = transverse flange moment per unit length of double tee

$m_{f,max}$ = maximum flange moment per unit length of double tee

n_{tf} = number of flange thicknesses by which web height is increased in computing J_w

r = variable in Eq. (23)

REO_k = rigid end offset factor for stiffness

REO_m = rigid end offset factor for moment

s = center to center web spacing

t = thickness of cross-section component

t_f = flange thickness

t_w = thickness of web

$t_{w,ave}$ = average thickness of web

$t_{w,bot}$ = thickness of web at bottom of web

$t_{w,top}$ = thickness of web at top of web

T = torque

T_t = total torque

T_{SV} = St. Venant torque

T_{SVw} = St. Venant torque in one web

T_{RW} = restraint-of-warping torque

u = variable in Eq. (23)

u_y = difference in vertical displacement between two webs

w = variable in Eq. (23)

W = weight of member

y = vector of unknown twist angles in finite difference solution

z = longitudinal coordinate

Δ = deflection of one web relative to the other, parallel to plane of web

η = variable in equation for $\phi_r(z)$

θ = variable in procedure for evaluating $\tanh(\eta L/2)$ when η is imaginary

λ = variable in equation for $\phi_r(z)$

μ = absolute value of ϱ

ν = variable in equation for $\phi_r(z)$

ν_c = Poisson's ratio for concrete

ϱ = dimensionless variable in equation for $\phi_r(z)$

σ_f = normal stress in flange due to bending

ϕ = twist angle

ϕ_0 = twist angle of one end of member relative to the other end

$\phi_{0,add}$ = additional twist angle of one end of member relative to the other end due to cross-section distortion

$\phi_{0,SV}$ = twist angle of one end of member relative to the other end when pure St. Venant behavior is assumed

ϕ_d = twist angle due to distortion of cross section

ϕ_r = twist angle due to rigid body rotation of cross section

ϕ_t = total twist angle

ϕ_{BL} = twist angle at bottom loaded node in FE analysis

ϕ_{BS} = twist angle at bottom supported node in FE analysis

ϕ_{TL} = twist angle at top loaded node in FE analysis

ϕ_{TS} = twist angle at top supported node in FE analysis

Φ = vector of nodal twist angles in FD analysis

ζ_k = constant associated with rigid end offset for stiffness

ζ_m = constant associated with rigid end offset for moment